

How Reliable is Your Regression Model's Uncertainty Under Real-World Distribution Shifts?

Fredrik K. Gustafsson

*Department of Information Technology
Uppsala University, Sweden*

Martin Danelljan

*Computer Vision Lab
ETH Zürich, Switzerland*

Thomas B. Schön

*Department of Information Technology
Uppsala University, Sweden*

Abstract

Many important computer vision applications are naturally formulated as regression problems. Within medical imaging, accurate regression models have the potential to automate various tasks, helping to lower costs and improve patient outcomes. Such safety-critical deployment does however require reliable estimation of model uncertainty, also under the wide variety of distribution shifts that might be encountered in practice. Motivated by this, we set out to investigate the reliability of regression uncertainty estimation methods under various real-world distribution shifts. To that end, we propose an extensive benchmark of 8 image-based regression datasets with different types of challenging distribution shifts. We then employ our benchmark to evaluate many of the most common uncertainty estimation methods, as well as two state-of-the-art uncertainty scores from the task of out-of-distribution detection. We find that while methods are well calibrated when there is no distribution shift, they all become highly overconfident on many of the benchmark datasets. This uncovers important limitations of current uncertainty estimation methods, and the proposed benchmark therefore serves as a challenge to the research community. We hope that our benchmark will spur more work on how to develop truly reliable regression uncertainty estimation methods. Code is available at https://github.com/fregu856/regression_uncertainty.

1 Introduction

Regression is a fundamental machine learning problem with many important computer vision applications (Rothe et al., 2016; Law & Deng, 2018; Xiao et al., 2018; Zhu et al., 2018; Shi et al., 2019; Lathuilière et al., 2019). In general, it entails predicting continuous targets y from given inputs x . Within medical imaging, a number of tasks are naturally formulated as regression problems, including brain age estimation (Cole et al., 2017; Jónsson et al., 2019; Shi et al., 2020), prediction of cardiovascular volumes and risk factors (Xue et al., 2017; Poplin et al., 2018) and body composition analysis (Langner et al., 2020; 2021). If machine learning models could be deployed to automatically regress various such properties within real-world clinical practice, this would ultimately help lower costs and improve patient outcomes across the medical system (Topol, 2019).

Real-world deployment in medical applications, and within other safety-critical domains, does however put very high requirements on such regression models. In particular, the common approach of training a deep neural network (DNN) to directly output a predicted regression target $\hat{y} = f(x)$ is *not* sufficient, as it fails to capture any measure of uncertainty in the predictions \hat{y} . The model is thus unable to e.g. detect inputs x which are out-of-distribution (OOD) compared to its training data. Since the predictive accuracy of DNNs

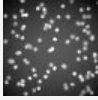
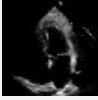
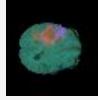
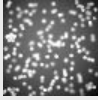
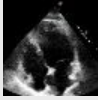
	Cells-Tails	ChairAngle-Gap	AssetWealth	Ventricular Volume	BrainTumour Pixels	SkinLesion Pixels	Histology NucleiPixels	AerialBuilding Pixels
Train								
	$y = 100$	$y = 80.5$	$y = 1.594$	$y = 40.38$	$y = 252$	$y = 500$	$y = 1257$	$y = 1097$
Test								
	$y = 198$	$y = 43.8$	$y = 1.314$	$y = 85.93$	$y = 273$	$y = 516$	$y = 1156$	$y = 433$

Figure 1: We propose a benchmark consisting of 8 image-based regression datasets, testing the reliability of regression uncertainty estimation methods under real-world distribution shifts. Example train (top row) and test inputs x , along with the corresponding ground truth targets y , are here shown for each of the 8 datasets.

typically degrades significantly on OOD inputs (Hendrycks & Dietterich, 2019; Koh et al., 2021), this could have potentially catastrophic consequences. Much research effort has therefore been invested into various approaches for training uncertainty-aware DNN models (Blundell et al., 2015; Gal, 2016; Kendall & Gal, 2017; Lakshminarayanan et al., 2017; Romano et al., 2019), to explicitly estimate the uncertainty in the predictions.

These uncertainty estimates must however be accurate and reliable. Otherwise, if the model occasionally becomes overconfident and outputs highly confident yet incorrect predictions, providing uncertainty estimates might just instill a false sense of security – arguably making the model even less suitable for safety-critical deployment. Specifically, the uncertainty estimates must be *well calibrated* and properly align with the prediction errors (Gneiting et al., 2007; Guo et al., 2017). Moreover, the uncertainty must remain well calibrated also under the wide variety of *distribution shifts* that might be encountered during practical deployment (Quionero-Candela et al., 2009; Finlayson et al., 2021). For example in medical applications, a model trained on data collected solely at a large urban hospital in the year 2020, for instance, should output well-calibrated predictions also in 2023, for patients both from urban and rural areas. While uncertainty calibration, as well as general DNN robustness (Hendrycks et al., 2021a), has been evaluated under distribution shifts for classification tasks (Ovadia et al., 2019), this important problem is not well-studied for *regression*.

Motivated by this, we set out to investigate the reliability of regression uncertainty estimation methods under various real-world distribution shifts. To that end, we propose an extensive benchmark consisting of 8 image-based regression datasets (see Figure 1) with different types of distribution shifts. These are all publicly available and relatively large-scale datasets (6 592 - 20 614 training images), yet convenient to store and train models on (64×64 images with 1D regression targets). Four of the datasets are also taken from medical applications, with clinically relevant distribution shifts. We evaluate some of the most commonly used regression uncertainty estimation methods, including conformal prediction, quantile regression and what is often considered the state-of-the-art – ensembling (Ovadia et al., 2019; Gustafsson et al., 2020b). We also consider the approach of selective prediction (Geifman & El-Yaniv, 2017), in which the regression model can abstain from outputting predictions for certain inputs. This enables us to evaluate uncertainty scores from the rich literature on OOD detection (Salehi et al., 2022). Specifically, we evaluate two recent scores based on feature-space density (Mukhoti et al., 2021a; Pleiss et al., 2020; Sun et al., 2022; Kuan & Mueller, 2022).

In total, we evaluate 10 different methods. Among them, we find that not a single one is close to being perfectly calibrated across all datasets. While the methods are well calibrated on baseline variants with no distribution shifts, they all become highly overconfident on many of our benchmark datasets. Also the conformal prediction methods suffer from this issue, despite their commonly promoted theoretical guarantees. This highlights the importance of always being aware of underlying assumptions, assessing whether or not they are likely to hold in practice. Methods based on the state-of-the-art OOD uncertainty scores perform well *relative* to other methods, but are also overconfident in many cases – the *absolute* performance is arguably

still not sufficient. Our proposed benchmark thus serves as a challenge to the research community, and we hope that it will spur more work on how to develop truly reliable regression uncertainty estimation methods.

Summary of Contributions We collect a set of 8 large-scale yet convenient image-based regression datasets with different types of challenging distribution shifts. Utilizing this, we propose a benchmark for testing the reliability of regression uncertainty estimation methods under real-world distribution shifts. We then employ our benchmark to evaluate many of the most common uncertainty estimation methods, as well as two state-of-the-art uncertainty scores from OOD detection. We find that all methods become highly overconfident on many of the benchmark datasets, thus uncovering limitations of current uncertainty estimation methods.

2 Background

In a regression problem, the task is to predict a target $y^* \in \mathcal{Y}$ for any given input $x^* \in \mathcal{X}$. To solve this, we are also given a train set of i.i.d. input-target pairs, $\mathcal{D}_{\text{train}} = \{(x_i, y_i)\}_{i=1}^N, (x_i, y_i) \sim p(x, y)$. What separates regression from classification is that the target space \mathcal{Y} is continuous, $\mathcal{Y} = \mathbb{R}^K$. In this work, we only consider the 1D case, i.e. when $\mathcal{Y} = \mathbb{R}$. Moreover, the input space \mathcal{X} here always corresponds to the space of images.

Prediction Intervals, Coverage & Calibration Given a desired miscoverage rate α , a *prediction interval* $C_\alpha(x^*) = [L_\alpha(x^*), U_\alpha(x^*)] \subseteq \mathbb{R}$ is a function that maps the input x^* onto an interval that should cover the true regression target y^* with probability $1 - \alpha$. For any set $\{(x_i^*, y_i^*)\}_{i=1}^{N^*}$ of N^* examples, the empirical interval *coverage* is the proportion of inputs for which the prediction interval covers the corresponding target,

$$\text{Coverage}(C_\alpha) = \frac{1}{N^*} \sum_{i=1}^{N^*} \mathbb{I}\{y_i^* \in C_\alpha(x_i^*)\}. \quad (1)$$

If the coverage equals $1 - \alpha$, we say that the prediction intervals are perfectly *calibrated*. Unless stated otherwise, we set $\alpha = 0.1$ in this work. The prediction intervals should thus obtain a coverage of 90%.

2.1 Regression Uncertainty Estimation Methods

The most common approach to image-based regression is to train a DNN $f_\theta : \mathcal{X} \rightarrow \mathbb{R}$ that outputs a predicted target $\hat{y} = f_\theta(x)$ for any input x , using e.g. the L2 or L1 loss (Lathuilière et al., 2019). We are interested in methods which extend this standard direct regression approach to also provide uncertainty estimates for the predictions. Specifically, we consider methods which output a prediction interval $C_\alpha(x)$ and a predicted target $\hat{y}(x) \in C_\alpha(x)$ for each input x . The uncertainty in the prediction $\hat{y}(x)$ is then quantified as the length of the interval $C_\alpha(x)$ (larger interval - higher uncertainty). Some of the most commonly used regression uncertainty estimation methods fall under this category, as described in more detail below.

Conformal Prediction The standard regression approach can be extended by utilizing the framework of split conformal prediction (Papadopoulos et al., 2002; Papadopoulos, 2008; Romano et al., 2019). This entails splitting the train set $\{(x_i, y_i)\}_{i=1}^N$ into a proper train set \mathcal{I}_1 and a calibration set \mathcal{I}_2 . The DNN f_θ is trained on \mathcal{I}_1 , and absolute residuals $R = \{|y_i - f_\theta(x_i)| : i \in \mathcal{I}_2\}$ are computed on the calibration set \mathcal{I}_2 . Given a new input x^* , a prediction interval $C_\alpha(x^*)$ is then constructed from the prediction $f_\theta(x^*)$ as,

$$C_\alpha(x^*) = [f_\theta(x^*) - Q_{1-\alpha}(R, \mathcal{I}_2), f_\theta(x^*) + Q_{1-\alpha}(R, \mathcal{I}_2)], \quad (2)$$

where $Q_{1-\alpha}(R, \mathcal{I}_2)$ is the $(1-\alpha)$ -th quantile of the absolute residuals R . Under the assumption of exchangeably drawn train and test data, this prediction interval is guaranteed to satisfy $\mathbb{P}\{y^* \in C_\alpha(x^*)\} \geq 1 - \alpha$ (marginal coverage guarantee). The interval $C_\alpha(x^*)$ has a fixed length of $2Q_{1-\alpha}(R, \mathcal{I}_2)$ for all inputs x^* .

Quantile Regression A DNN can also be trained to directly output prediction intervals of input-dependent length, utilizing the quantile regression approach (Koenker & Bassett Jr, 1978; Romano et al., 2019; Jensen et al., 2022). This entails estimating the conditional quantile function $q^\alpha(x) = \inf\{y \in \mathbb{R} : F_{Y|X}(y|x) \geq \alpha\}$, where $F_{Y|X}$ is the conditional cumulative distribution function. Specifically, a DNN is trained to output estimates of the lower and upper quantiles $q^{\alpha_{\text{lo}}}(x)$, $q^{\alpha_{\text{up}}}(x)$ at $\alpha_{\text{lo}} = \alpha/2$ and $\alpha_{\text{up}} = 1 - \alpha/2$. Given a new input x^* , a prediction interval $C_\alpha(x^*)$ can then be directly formed as,

$$C_\alpha(x^*) = [q_\theta^{\alpha_{\text{lo}}}(x^*), q_\theta^{\alpha_{\text{up}}}(x^*)]. \quad (3)$$

The estimated quantiles $q_\theta^{\alpha_{\text{lo}}}(x^*)$, $q_\theta^{\alpha_{\text{up}}}(x^*)$ can be output by a single DNN f_θ , trained using the pinball loss (Steinwart & Christmann, 2011). A prediction $\hat{y}(x^*)$ can also be extracted as the center point of $C_\alpha(x^*)$.

Probabilistic Regression Another approach is to explicitly model the conditional distribution $p(y|x)$, for example using a Gaussian model $p_\theta(y|x) = \mathcal{N}(y; \mu_\theta(x), \sigma_\theta^2(x))$ (Chua et al., 2018; Gustafsson et al., 2020a). A single DNN f_θ can be trained to output both the mean $\mu_\theta(x)$ and variance $\sigma_\theta^2(x)$ by minimizing the corresponding negative log-likelihood. For a given input x^* , a prediction interval can then be constructed as,

$$C_\alpha(x^*) = [\mu_\theta(x^*) - \sigma_\theta(x^*)\Phi^{-1}(1 - \alpha/2), \mu_\theta(x^*) + \sigma_\theta(x^*)\Phi^{-1}(1 - \alpha/2)], \quad (4)$$

where Φ is the CDF of the standard normal distribution. The mean $\mu_\theta(x^*)$ is also taken as a prediction \hat{y} .

Epistemic Uncertainty From the Bayesian perspective, quantile regression and Gaussian models capture aleatoric (inherent data noise) but not epistemic uncertainty, which accounts for uncertainty in the model parameters (Gal, 2016; Kendall & Gal, 2017). This can be estimated in a principled manner via Bayesian inference, and various approximate methods have been explored (Neal, 1995; Ma et al., 2015; Blundell et al., 2015; Gal & Ghahramani, 2016). In practice, it has been shown difficult to beat the simple approach of ensembling (Lakshminarayanan et al., 2017; Ovadia et al., 2019), which entails training M models $\{f_{\theta_i}\}_{i=1}^M$ and combining their predictions. For Gaussian models, a single mean $\hat{\mu}$ and variance $\hat{\sigma}^2$ can be computed as,

$$\hat{\mu}(x^*) = \frac{1}{M} \sum_{i=1}^M \mu_{\theta_i}(x^*), \quad \hat{\sigma}^2(x^*) = \frac{1}{M} \sum_{i=1}^M \left((\hat{\mu}(x^*) - \mu_{\theta_i}(x^*))^2 + \sigma_{\theta_i}^2(x^*) \right), \quad (5)$$

and then plugged into (4) to construct a prediction interval $C_\alpha(x^*)$ for a given input x^* .

2.2 Selective Prediction

The framework of selective prediction has been applied both to classification (Herbei & Wegkamp, 2006; Geifman & El-Yaniv, 2017) and regression problems (Jiang et al., 2020). The general idea is to give a model the option to abstain from outputting predictions for some inputs. This is achieved by combining the prediction model f_θ with an uncertainty function $\kappa_f : \mathcal{X} \rightarrow \mathbb{R}$. Given an input x^* , the prediction $f_\theta(x^*)$ is output if the uncertainty $\kappa_f(x^*) \leq \tau$ (for some user-specified threshold τ), otherwise x^* is rejected and no prediction is made. The *prediction rate* is the proportion of inputs for which a prediction is output,

$$\text{Prediction Rate} = \frac{1}{N^*} \sum_{i=1}^{N^*} \mathbb{I}\{\kappa_f(x_i^*) \leq \tau\}. \quad (6)$$

In principle, if high uncertainty $\kappa_f(x^*)$ corresponds to a large prediction error $|y^* - \hat{y}(x^*)|$ and vice versa, small errors will be achieved for all predictions which are actually output by the model. Specifically in this work, we combine selective prediction with the regression methods from Section 2.1. A prediction interval $C_\alpha(x^*)$ and predicted target $\hat{y}(x^*)$ are thus output if and only if (iff) $\kappa_f(x^*) \leq \tau$. Our aim is for this to improve the calibration (interval coverage closer to $1 - \alpha$) of the output prediction intervals.

For the uncertainty function $\kappa_f(x)$, the variance $\hat{\sigma}^2(x)$ of a Gaussian ensemble (5) could be used, for example. One could also use some of the various uncertainty scores employed in the rich OOD detection literature (Salehi et al., 2022). In OOD detection, the task is to distinguish in-distribution inputs x , inputs which are similar to those of the train set $\{(x_i, y_i)\}_{i=1}^N$, from out-of-distribution inputs. A principled approach to OOD detection would be to fit a model of $p(x)$ on the train set. Inputs x for which $p(x)$ is small are then deemed OOD (Serrà et al., 2020). In our considered case where inputs x are images, modelling $p(x)$ can however be quite challenging. To mitigate this, a feature extractor $g : \mathcal{X} \rightarrow \mathbb{R}^{D_g}$ can be utilized, modelling $p(x)$ indirectly by fitting a simple model to the feature vectors $g(x)$. In the classification setting, Mukhoti et al. (2021a) fit a Gaussian mixture model (GMM) to the feature vectors $\{g(x_i)\}_{i=1}^N$ of the train set. Given an input x^* , it is then deemed OOD if the GMM density $\text{GMM}(g(x^*))$ is small. Pleiss et al. (2020) apply this approach also to regression problems. Instead of fitting a GMM to the feature vectors and evaluating its density, (Sun et al., 2022; Kuan & Mueller, 2022) compute the distance $\text{kNN}(g(x^*))$ between $g(x^*)$ and its k nearest neighbors in the train set $\{g(x_i)\}_{i=1}^N$. The input x^* is then deemed OOD if this kNN distance is large.

3 Proposed Benchmark

We propose an extensive benchmark for testing the reliability of regression uncertainty estimation methods under real-world distribution shifts. The benchmark consists of 8 publicly available image-based regression datasets, which are described in detail in Section 3.1. Our complete evaluation procedure, evaluating uncertainty estimation methods mainly in terms of prediction interval coverage, is then described in Section 3.2.

3.1 Datasets

In an attempt to create a standard benchmark for image-based regression under distribution shifts, we collect and modify 8 datasets from the literature. Two of them contain synthetic images while the remaining six are real-world datasets, four of which are taken from medical applications. Examples from each of the 8 datasets are shown in Figure 1. We create two additional variants of each of the synthetic datasets, thus resulting in 12 datasets in total. They are all relatively large-scale (6 592 - 20 614 train images) and contain input images x of size 64×64 along with 1D regression targets y . Descriptions of all 12 datasets are given below (further details are also provided in Appendix A), starting with the two synthetic datasets and their variants.

Cells Given a synthetic fluorescence microscopy image x , the task is to predict the number of cells y in the image. We utilize the Cell-200 dataset from Ding et al. (2021; 2020), consisting of 200 000 grayscale images of size 64×64 . We randomly draw 10 000 train images, 2 000 val images and 10 000 test images. Thus, there is no distribution shift between train/val and test. We therefore use this as a baseline dataset.

Cells-Tails A variant of CELLS with a clear distribution shift between train/val and test. For train/val, the regression targets y are limited to $]50, 150]$. For test, the targets instead lie in the original range $[1, 200]$.

Cells-Gap Another variant of CELLS with a clear distribution shift between train/val and test. For train/val, the regression targets y are limited to $[1, 50] \cup [150, 200]$. For test, the targets instead lie in the original $[1, 200]$.

ChairAngle Given a synthetic image x of a chair, the task is to predict the yaw angle y of the chair. We utilize the RC-49 dataset (Ding et al., 2021; 2020), which contains 64×64 images of different chair models rendered at yaw angles ranging from 0.1° to 89.9° . We randomly split their training set and obtain 17 640 train images and 4 410 val images. By sub-sampling their test set we also get 11 225 test images. There is no clear distribution shift between train/val and test, and we therefore use this as a second baseline dataset.

ChairAngle-Tails A variant of CHAIRANGLE with a clear distribution shift between train/val and test. For train/val, we limit the regression targets y to $]15, 75[$. For test, the targets instead lie in the original $]0, 90[$.

ChairAngle-Gap Another variant of CHAIRANGLE with a clear distribution shift. For train/val, the regression targets y are limited to $]0, 30] \cup [60, 90[$. For test, the targets instead lie in the original $]0, 90[$.

AssetWealth Given a satellite image x , the task is to predict the asset wealth index y of the region. We utilize the PovertyMap-Wilds dataset from (Koh et al., 2021), which is a variant of the dataset collected by Yeh et al. (2020). We use the training, validation-ID and test-OOD subsets of the data, giving us 9 797 train images, 1 000 val images and 3 963 test images. We resize the images from size 224×224 to 64×64 . Train/val and test contain satellite images from disjoint sets of African countries, creating a distribution shift.

VentricularVolume Given an echocardiogram image x of a human heart, the task is to predict the volume y of the left ventricle. We utilize the EchoNet-Dynamic dataset (Ouyang et al., 2020), which contains 10 030 echocardiogram videos. Each video captures a complete cardiac cycle and is labeled with the left ventricular volume at two separate time points, representing end-systole (at the end of contraction) and end-diastole (just before contraction). For each video, we extract just one of these volume measurements along with the corresponding video frame. To create a clear distribution shift between train/val and test, we select the end systolic volume (smaller volume) for train and val, but the end diastolic volume (larger volume) for test. We utilize the provided dataset splits, giving us 7 460 train images, 1 288 val images and 1 276 test images.

BrainTumourPixels Given an image slice x of a brain MRI scan, the task is to predict the number of pixels y in the image which are labeled as brain tumour. We utilize the brain tumour dataset of the medical segmentation decathlon (Simpson et al., 2019; Antonelli et al., 2022), which is a subset of the data used in

the 2016 and 2017 BraTS challenges (Bakas et al., 2018; 2017; Menze et al., 2014). The dataset contains 484 brain MRI scans with corresponding tumour segmentation masks. We split these scans 80%/20%/20% into train, val and test sets. The scans are 3D volumes of size $240 \times 240 \times 155$. We convert each scan into 155 image slices of size 240×240 , and create a regression target for each image by counting the number of labeled brain tumour pixels. This gives us 20 614 train images, 6 116 val images and 6 252 test images.

SkinLesionPixels Given a dermatoscopic image x of a pigmented skin lesion, the task is to predict the number of pixels y in the image which are labeled as lesion. We utilize the HAM10000 dataset by Tschandl et al. (2018), which contains 10 015 dermatoscopic images with corresponding skin lesion segmentation masks. HAM10000 consists of four different sub-datasets, three of which were collected in Austria, while the fourth sub-dataset was collected in Australia. To create a clear distribution shift between train/val and test, we use the Australian sub-dataset as our test set. After randomly splitting the remaining images 85%/15% into train and val sets, we obtain 6 592 train images, 1 164 val images and 2 259 test images.

HistologyNucleiPixels Given an H&E stained histology image x , the task is to predict the number of pixels y in the image which are labeled as nuclei. We utilize the CoNSeP dataset by Graham et al. (2019), along with the pre-processed versions they provide of the Kumar (Kumar et al., 2017) and TNBC (Naylor et al., 2018) datasets. The datasets contain large H&E stained image tiles, with corresponding nuclear segmentation masks. The three datasets were collected at different hospitals/institutions, with differing procedures for specimen preservation and staining. By using CoNSeP and Kumar for train/val and TNBC for test, we thus obtain a clear distribution shift. From the large image tiles, we extract 64×64 patches via regular gridding, and create a regression target for each image patch by counting the number of labeled nuclei pixels. In the end, we obtain 10 808 train images, 2 702 val images and 2 267 test images.

AerialBuildingPixels Given an aerial image x , the task is to predict the number of pixels y in the image which are labeled as building. We utilize the Inria aerial image labeling dataset (Maggiori et al., 2017), which contains 180 large aerial images with corresponding building segmentation masks. The images are captured at five different geographical locations. We use the images from two densely populated American cities for train/val, and the images from a more rural European area for test, thus obtaining a clear distribution shift. After preprocessing, we obtain 11 184 train images, 2 797 val images and 3 890 test images.

3.2 Evaluation

We propose to evaluate regression uncertainty estimation methods mainly in terms of prediction interval coverage (1): if a method outputs a prediction $\hat{y}(x)$ and a 90% prediction interval $C_{0.1}(x)$ for each input x , does the method actually achieve 90% coverage on the *test* set? I.e., are the prediction intervals calibrated?

Motivation Regression uncertainty estimation methods can be evaluated using various approaches. One alternative is sparsification (Ilg et al., 2018), measuring how well the uncertainty can be used to sort predictions from worst to best. Perfect sparsification can however be achieved even if the absolute scale of the uncertainty is consistently underestimated. Therefore, a lot of previous work has instead evaluated methods in terms of calibration (Gneiting et al., 2007; Guo et al., 2017). Specifically for regression, a common form of calibration is based on quantiles (Kuleshov et al., 2018; Cui et al., 2020; Chung et al., 2021). Essentially, a model is said to be calibrated if the interval coverage (1) equals $1 - \alpha$ for *all* miscoverage rates $\alpha \in]0, 1[$. This is measured by the expected calibration error, $\text{ECE} = \frac{1}{m} \sum_{j=1}^m |\text{Coverage}(C_{\alpha_j}) - (1 - \alpha_j)|$, $\alpha_j \sim \text{U}(0, 1)$. Our proposed evaluation metric is thus a special case of this approach, considering just one specific miscoverage rate $\alpha = 0.1$. We argue that this results in a simpler and more interpretable metric, which also is motivated by how prediction intervals actually are used in real-world applications. There, one particular value of α is selected ($\alpha = 0.1$ is a common choice), and the corresponding intervals C_α are then expected to achieve a coverage of $1 - \alpha$ on unseen test data. Recent alternative calibration metrics directly measure how well the uncertainty aligns with the prediction errors (Levi et al., 2022; Pickering & Sapsis, 2022). While these enable relative comparisons of different methods, they are not easily interpretable in terms of absolute performance.

Implementation Details For each dataset and method, we first train a DNN on the train set $\mathcal{D}_{\text{train}}$. Then, we run the method on the *val* set \mathcal{D}_{val} , resulting in a prediction interval $C_\alpha(x) = [L_\alpha(x), U_\alpha(x)]$ for each input x ($\alpha = 0.1$). Importantly, we then calibrate these prediction intervals on *val* using the procedure in (Romano et al., 2019). This gives calibrated prediction intervals $\tilde{C}_\alpha(x)$, for which the interval coverage on *val*

exactly equals $1 - \alpha$. Specifically, $\tilde{C}_\alpha(x)$ is constructed from the original interval $C_\alpha(x) = [L_\alpha(x), U_\alpha(x)]$,

$$\tilde{C}_\alpha(x) = [L_\alpha(x) - Q_{1-\alpha}(E, \mathcal{D}_{\text{val}}), U_\alpha(x) + Q_{1-\alpha}(E, \mathcal{D}_{\text{val}})], \quad (7)$$

where $E = \{\max(L_\alpha(x_i) - y_i, y_i - U_\alpha(x_i)) : i \in \mathcal{D}_{\text{val}}\}$ are conformity scores computed on \mathcal{D}_{val} , and $Q_{1-\alpha}(E, \mathcal{D}_{\text{val}})$ is the $(1 - \alpha)$ -th quantile of these scores. Finally, we then run the method on the test set $\mathcal{D}_{\text{test}}$, outputting a calibrated prediction interval $\tilde{C}_\alpha(x^*)$ for each input x^* . Ideally, the interval coverage of $\tilde{C}_\alpha(x^*)$ does not change from val to test, i.e. $\text{Coverage}(\tilde{C}_\alpha) = 1 - \alpha$ should be true also on test. If $\text{Coverage}(\tilde{C}_\alpha) \neq 1 - \alpha$, a conservative method ($> 1 - \alpha$) is preferred compared to an *overconfident* method ($< 1 - \alpha$). For methods based on selective prediction (Section 2.2), the only difference is that prediction intervals $\tilde{C}_\alpha(x^*)$ are output only for some test inputs x^* (iff $\kappa_f(x^*) \leq \tau$). The interval coverage is thus computed only on this subset of test. We set $\alpha = 0.1$ since this is a commonly used miscoverage rate in practice.

Secondary Metrics We also evaluate methods in terms of mean absolute error (MAE) and average interval length on the *val* set. This measures the quality of the prediction $\hat{y}(x)$ and the prediction interval $C_\alpha(x)$, respectively. A method that achieves a coverage close to $1 - \alpha$, but outputs extremely large intervals for all inputs x , would still not be particularly useful in practice. For methods based on selective prediction, we also evaluate in terms of the prediction rate (6) on test. If a coverage close to $1 - \alpha$ is achieved with a very low prediction rate, the method might still not be practically useful in certain applications.

4 Evaluated Methods

We evaluate five common regression uncertainty estimation methods from Section 2.1, which all output a prediction interval $C_\alpha(x)$ and a predicted target $\hat{y}(x) \in C_\alpha(x)$ for each input x . Two of these we also combine with selective prediction (Section 2.2), utilizing four different uncertainty functions $\kappa_f(x)$. In total, we evaluate 10 different methods. For all methods, we train models based on a ResNet34 (He et al., 2016) backbone DNN. This architecture is chosen because of its simplicity and widespread use. The ResNet takes an image x as input and outputs a feature vector $g(x) \in \mathbb{R}^{512}$. Below we specify and provide implementation details for each of the 10 evaluated methods, while we refer back to Section 2 for more general descriptions.

Conformal Prediction We create a standard direct regression model by feeding the ResNet feature vector $g(x)$ into a network head of two fully-connected layers, outputting a scalar prediction $f_\theta(x)$. The model is trained using the L2 loss. We then utilize conformal prediction to create prediction intervals $C_\alpha(x)$ according to (2). Instead of splitting the train images into \mathcal{I}_1 and \mathcal{I}_2 , we use the val images as the calibration set \mathcal{I}_2 .

Ensemble We train an ensemble $\{f_{\theta_1}, \dots, f_{\theta_M}\}$ of $M = 5$ direct regression models and compute the ensemble mean $\hat{\mu}(x) = \frac{1}{M} \sum_{i=1}^M f_{\theta_i}(x)$ and ensemble variance $\hat{\sigma}^2(x) = \frac{1}{M} \sum_{i=1}^M (\hat{\mu}(x) - f_{\theta_i}(x))^2$. By inserting these into equation 4, prediction intervals $C_\alpha(x)$ of input-dependent length are then constructed.

Gaussian We create a Gaussian model $p_\theta(y|x) = \mathcal{N}(y; \mu_\theta(x), \sigma_\theta^2(x))$ by feeding the ResNet feature vector $g(x)$ into two separate network heads of two fully-connected layers. These output the mean $\mu_\theta(x)$ and variance $\sigma_\theta^2(x)$, respectively. Prediction intervals $C_\alpha(x)$ are then constructed according to (4).

Gaussian Ensemble We train an ensemble of $M = 5$ Gaussian models, compute a single mean $\hat{\mu}(x)$ and variance $\hat{\sigma}^2(x)$ according to (5), and plug these into (4) to construct prediction intervals $C_\alpha(x)$.

Quantile Regression We create a quantile regression model by feeding the ResNet feature vector $g(x)$ into two separate network heads. These output the quantiles $q_\theta^{\alpha_{\text{lo}}}(x), q_\theta^{\alpha_{\text{up}}}(x)$, directly forming prediction intervals $C_\alpha(x)$ according to (3). The model is trained by minimizing the average pinball loss of $q_\theta^{\alpha_{\text{lo}}}(x)$ and $q_\theta^{\alpha_{\text{up}}}(x)$.

Gaussian + Selective GMM We combine the GAUSSIAN method with a selective prediction mechanism. After training a Gaussian model, we run it on each image in train to extract ResNet feature vectors $\{g(x_i)\}_{i=1}^N$. We then utilize scikit-learn (Pedregosa et al., 2011) to fit a GMM (4 components, full covariance) to these train feature vectors. To compute an uncertainty score $\kappa_f(x)$ for a given input x , we extract $g(x)$ and evaluate its likelihood according to the fitted GMM, $\kappa_f(x) = -\text{GMM}(g(x))$. The prediction $\mu_\theta(x)$ and corresponding prediction interval $C_\alpha(x)$ of the Gaussian model are then output iff $\kappa_f(x) \leq \tau$. To set the user-specified threshold τ , we compute $\kappa_f(x)$ on all images in val and pick the 95% quantile. This choice of τ is motivated by the commonly reported FPR95 OOD detection metric, but τ could be set using other approaches.

Gaussian + Selective kNN Identical to GAUSSIAN + SELECTIVE GMM, but $\kappa_f(x) = \text{kNN}(g(x))$. Specifically, the uncertainty score $\kappa_f(x)$ is computed by extracting $g(x)$ and computing the average distance to its $k = 10$ nearest neighbors among the train feature vectors $\{g(x_i)\}_{i=1}^N$. Following Kuan & Mueller (2022), we utilize the Annoy¹ approximate neighbors library, with cosine similarity as the distance metric.

Gaussian + Selective Variance Identical to GAUSSIAN + SELECTIVE GMM, but $\kappa_f(x) = \sigma_\theta^2(x)$ (the variance of the Gaussian model). This is used as a simple baseline for the two previous methods.

Gaussian Ensemble + Selective GMM We combine GAUSSIAN ENSEMBLE with a selective prediction mechanism. After training an ensemble of $M = 5$ Gaussian models, we run each model on each image in train to extract M sets of ResNet feature vectors. For each model, we then fit a GMM to its set of train feature vectors. I.e., we fit M different GMMs. To compute an uncertainty score $\kappa_f(x)$ for a given input x , we extract a feature vector and evaluate its likelihood according to the corresponding GMM, for each of the M models. Finally, we compute the mean of the GMM likelihoods, $\kappa_f(x) = \frac{1}{M} \sum_{i=1}^M -\text{GMM}_i(g_i(x))$.

Gaussian Ensemble + Selective Ensemble Variance Identical to GAUSSIAN ENSEMBLE + SELECTIVE GMM, but $\kappa_f(x) = \frac{1}{M} \sum_{i=1}^M (\hat{\mu}(x) - \mu_{\theta_i}(x))^2$, where $\hat{\mu}(x) = \frac{1}{M} \sum_{i=1}^M \mu_{\theta_i}(x)$. Hence, the variance of the ensemble means is used as the uncertainty score. This constitutes a simple baseline for the previous method.

All models are trained for 75 epochs using the ADAM optimizer (Kingma & Ba, 2014). The same hyperparameters are used for all datasets, and neither the training procedure nor the models are specifically tuned for any particular dataset. All experiments are implemented using PyTorch (Paszke et al., 2019), and our complete implementation is made publicly available. All models were trained on individual NVIDIA TITAN Xp GPUs. On one such GPU, training 20 models on one dataset took approximately 24 hours.

5 Related Work

Out-of-distribution robustness of DNNs is an active area of research (Hendrycks & Dietterich, 2019; Hendrycks et al., 2021b;a; Izmailov et al., 2021; Yao et al., 2022; Schwinn et al., 2022; Wiles et al., 2022; Zhang et al., 2022). All these previous works do however focus exclusively on *classification* tasks. Moreover, they consider no uncertainty measures but instead evaluate only in terms of accuracy. While (Zaidi et al., 2021; Hendrycks et al., 2022) evaluate uncertainty calibration, they also just consider the classification setting. In contrast, evaluation of uncertainty estimation methods is our main focus, and we do this specifically for *regression*.

The main sources of inspiration for our work are (Koh et al., 2021) and (Ovadia et al., 2019). While Koh et al. (2021) propose an extensive benchmark with various real-world distribution shifts, it only contains a single regression dataset. Moreover, methods are evaluated solely in terms of predictive performance. Ovadia et al. (2019) perform a comprehensive evaluation of uncertainty estimation methods under distribution shifts, but only consider classification tasks. Inspired by this, we thus propose our benchmark for evaluating reliability of *uncertainty estimation* methods under *real-world distribution shifts* in the *regression* setting. Most similar to our work is that of Malinin et al. (2021). However, their benchmark contains just two regression datasets (tabular weather prediction and a complex vehicle motion prediction task), they only evaluate ensemble-based uncertainty estimation methods, and these methods are not evaluated in terms of calibration.

6 Results

We evaluate the 10 methods specified in Section 4 on all 12 datasets from Section 3.1, according to the evaluation procedure described in Section 3.2. For each method we train 20 models, randomly select 5 of them for evaluation and report the averaged metrics. For the ensemble methods, we construct an ensemble by randomly selecting $M = 5$ out of the 20 trained models, evaluate the ensemble and then repeat this 5 times in total. To ensure that the results do not depend on our specific choice of $\alpha = 0.1$, we also evaluate methods with two alternative miscoverage rates ($\alpha = 0.2$ and $\alpha = 0.05$) in Appendix B.

¹<https://github.com/spotify/annoy>

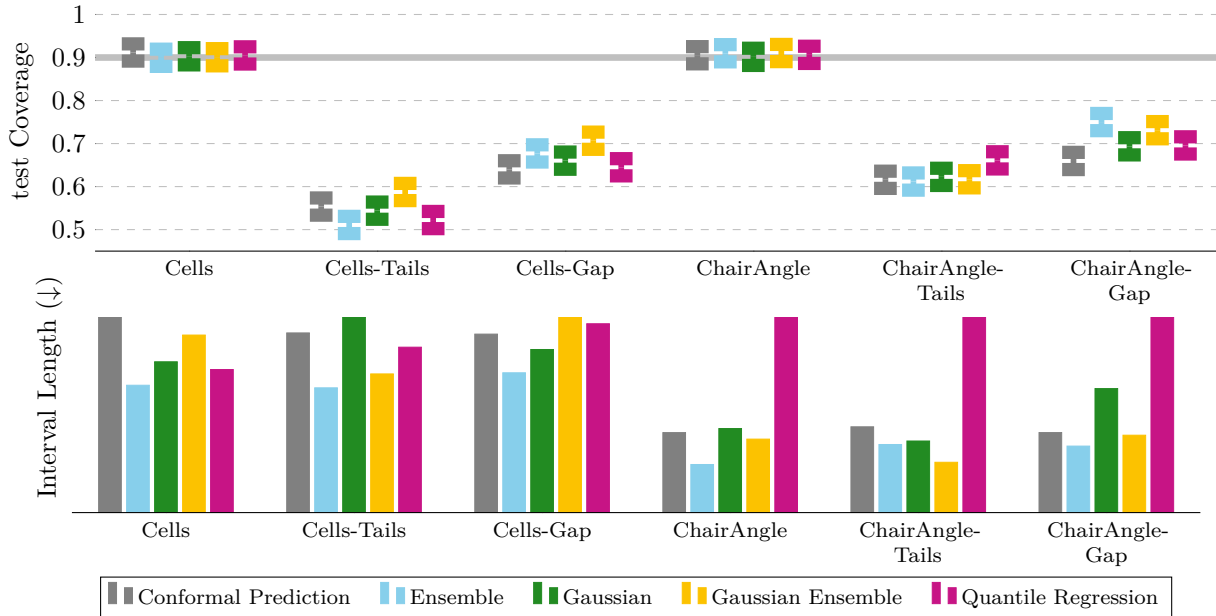


Figure 2: Results for the common regression uncertainty estimation methods, on the synthetic datasets.

6.1 Common Uncertainty Estimation Methods

We start by evaluating the first five methods from Section 4, those which output predictions and corresponding 90% prediction intervals for all inputs. The results in terms of our main metric test coverage are presented in the upper part of Figure 2 for the synthetic datasets, and in Figure 3 for the six real-world datasets. In the lower parts of Figure 2 & 3, results in terms of average val interval length are presented. The complete results, including our other secondary metric val MAE, are provided in Table A1 - Table A12 in the appendix.

In Figure 2, the test coverage results on the first synthetic dataset CELLS are found in the upper-left. As there is no distribution shift between train/val and test for this dataset, we use it as a baseline. We observe that all five methods have almost perfectly calibrated prediction intervals, i.e. they all obtain a test coverage very close to 90%. This is exactly the desired behaviour. On CELLS-TAILS however, on which we introduced a clear distribution shift, we observe in Figure 2 that the test coverage drops dramatically from the desired 90% for all five methods. Even the state-of-the-art uncertainty estimation method GAUSSIAN ENSEMBLE here becomes highly overconfident, as its test coverage drops down to $\approx 59\%$. On CELLS-GAP, the test coverages are slightly closer to 90%, but all five methods are still highly overconfident. On the other synthetic dataset CHAIRANGLE, we observe in Figure 2 that all five methods have almost perfectly calibrated prediction intervals. However, as we introduce clear distribution shifts on CHAIRANGLE-TAILS and CHAIRANGLE-GAP, we can observe that the test coverage once again drops dramatically for all methods.

The results on the six real-world datasets are found in Figure 3. In the upper part, we observe that all five methods have quite well-calibrated prediction intervals on ASSETWEALTH and BRAINTUMOURPIXELS, even though they all are consistently somewhat overconfident (test coverages of 82%-89%). On the four remaining datasets, the methods are in general more significantly overconfident. On VENTRICULARVOLUME, we observe test coverages of 60%-80% for all methods, and on SKINLESIONPIXELS the very best coverage is $\approx 82\%$. On HISTOLOGYNUCLEIPIXELS, most methods only obtain test coverages of 55%-70%, and on AERIALBUILDINGPIXELS the very best coverage is $\approx 81\%$. In fact, not a single method actually reaches the desired 90% test coverage on any of these real-world datasets.

In terms of average val interval length, we observe in the lower parts of Figure 2 & 3 that ENSEMBLE consistently produces smaller prediction intervals than CONFORMAL PREDICTION. Moreover, the intervals of GAUSSIAN ENSEMBLE are usually smaller than those of GAUSSIAN. When comparing the interval lengths of QUANTILE REGRESSION and GAUSSIAN, we observe no clear trend that is consistent across all datasets.

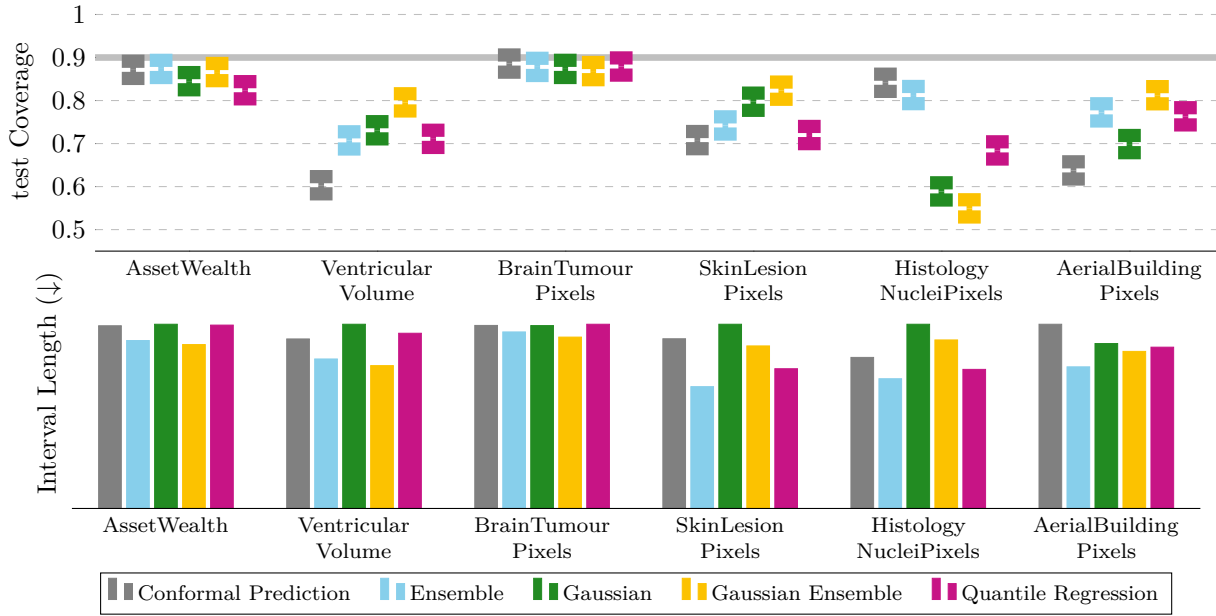


Figure 3: Results for the common regression uncertainty estimation methods, on the real-world datasets.

Since the average interval lengths vary a lot between different datasets, Figure 2 & 3 only show relative comparisons of the methods. For absolute numerical scales, see Table A1 - Table A12.

6.2 Selective Prediction Methods

Next, we evaluate the methods with an added selective prediction mechanism. We start with the three methods based on GAUSSIAN. The results in terms of test coverage and test prediction rate are available in Figure 4 for the synthetic datasets, and in Figure 5 for the six real-world datasets. Complete numerical results are also provided in Table A1 - Table A12 in the appendix.

In the upper part of Figure 4, we observe that selective prediction based on feature-space density significantly improves the test coverage of GAUSSIAN on the synthetic datasets. While GAUSSIAN has well-calibrated prediction intervals only on CELLS and CHAIRANGLE, which are baseline datasets without any distribution shift, GAUSSIAN + SELECTIVE GMM is almost perfectly calibrated across all six datasets. On CELLS-TAILS, for example, it improves the test coverage from $\approx 54\%$ up to $\approx 89\%$. GAUSSIAN + SELECTIVE kNN also significantly improves the test coverages, but not quite to the same extent. In the lower part of Figure 4, we can observe that when GAUSSIAN + SELECTIVE GMM significantly improves the test coverage, there is also a clear drop in its test prediction rate. For example, the prediction rate drops from ≈ 0.95 on CELLS down to ≈ 0.54 on CELLS-TAILS. By rejecting nearly 50% of all inputs as OOD in this case, GAUSSIAN + SELECTIVE GMM can thus remain well-calibrated on the subset of test it actually outputs predictions for. In Figure 4, we also observe that GAUSSIAN + SELECTIVE VARIANCE only marginally improves the test coverage.

While GAUSSIAN + SELECTIVE GMM significantly improves the test coverage of GAUSSIAN and has well-calibrated prediction intervals across the synthetic datasets, we observe in Figure 5 that this is not true for the six real-world datasets. GAUSSIAN + SELECTIVE GMM does consistently improve the test coverage, but only marginally, and it still suffers from significant overconfidence in many cases. On VENTRICULARVOLUME, for example, the test prediction rate of GAUSSIAN + SELECTIVE GMM is as low as ≈ 0.71 , but the test coverage only improves from $\approx 73\%$ to $\approx 75\%$ compared to GAUSSIAN. For the two methods based on GAUSSIAN ENSEMBLE, the results are presented in Figure A1 & A2 in the appendix. Overall, we observe very similar trends. GAUSSIAN ENSEMBLE + SELECTIVE GMM significantly improves the test coverage of GAUSSIAN ENSEMBLE and is almost perfectly calibrated across the synthetic datasets. However, when it comes to the real-world datasets, it often remains significantly overconfident.

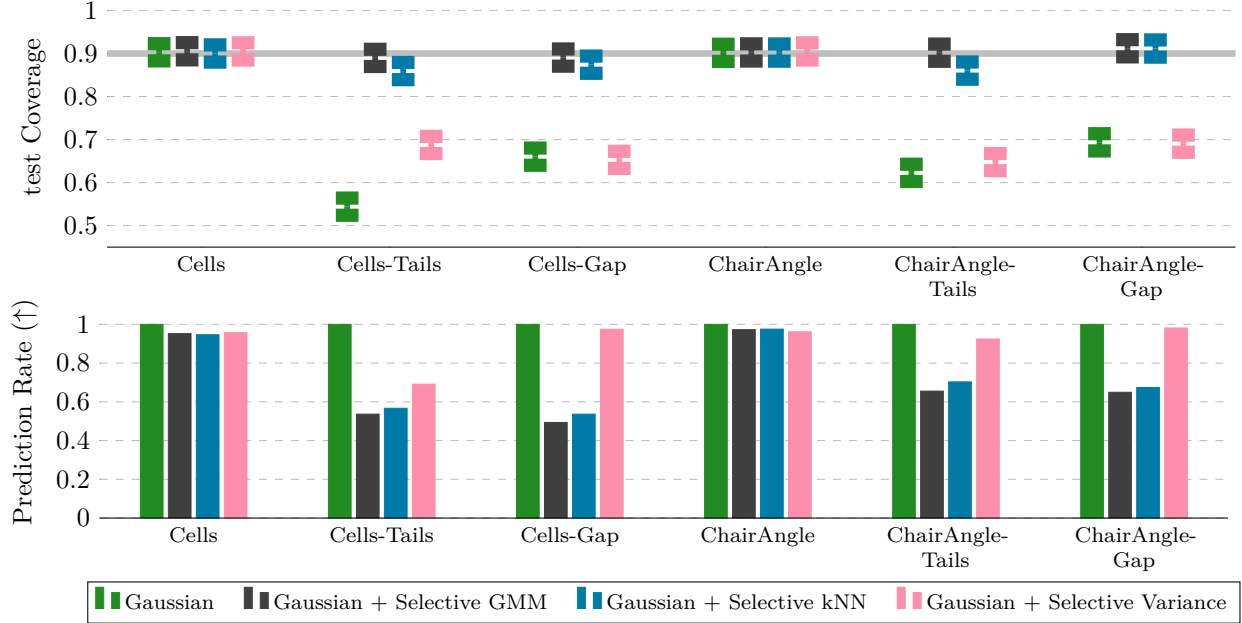


Figure 4: Results for the selective prediction methods based on GAUSSIAN, on the synthetic datasets.

6.3 Discussion

Let us now analyze the results from Section 6.1 & 6.2 in more detail, and discuss what we consider the most important findings and insights. First of all, we can observe that among the 10 considered methods, not a single one was close to producing perfectly calibrated prediction intervals across all 12 datasets. We thus conclude that our proposed benchmark indeed is challenging and interesting. Moreover, the results in Figure 2 & 3 demonstrate that while common uncertainty estimation methods are well calibrated when there is no distribution shift (CELLS and CHAIRANGLE), they can all break down and become highly overconfident in many realistic scenarios. This highlights the importance of employing sufficiently realistic and thus challenging benchmarks when evaluating uncertainty estimation methods. Otherwise, we might be lead to believe that methods will be more reliable during practical deployment than they actually are.

Coverage Guarantees Might Instill a False Sense of Security We also emphasize that CONFORMAL PREDICTION and QUANTILE REGRESSION² have theoretical coverage guarantees, but still are observed to become highly overconfident for many datasets in Figure 2 & 3. Since the guarantees depend on the assumption that all data points are exchangeable (true for i.i.d. data, for instance), which generally does not hold under distribution shifts, these results should actually not be surprising. The results are however a good reminder that we always need to be aware of the underlying assumptions, and whether or not they are likely to hold in common practical applications. Otherwise, such theoretical guarantees might just instill a false sense of security, making us trust methods more than we actually should.

Clear Performance Differences between Synthetic and Real-World Datasets We find it interesting that selective prediction based on feature-space density, in particular GAUSSIAN + SELECTIVE GMM, works almost perfectly in terms of test coverage across the synthetic datasets (Figure 4), but fails to give significant improvements on the real-world datasets (Figure 5). The results on VENTRICULARVOLUME are particularly interesting, as the prediction rate drops quite a lot without significantly improving the test coverage. This means that while a relatively large proportion of the test inputs are deemed OOD and thus rejected by the method, the test coverage is barely improved. On the synthetic datasets, there is a corresponding improvement in test coverage whenever the prediction rate drops significantly (Figure 4). It is not clear why such an obvious performance difference between synthetic and real-world datasets is observed. One possible

²Since all prediction intervals are calibrated on val, we are using *Conformalized Quantile Regression* (Romano et al., 2019).

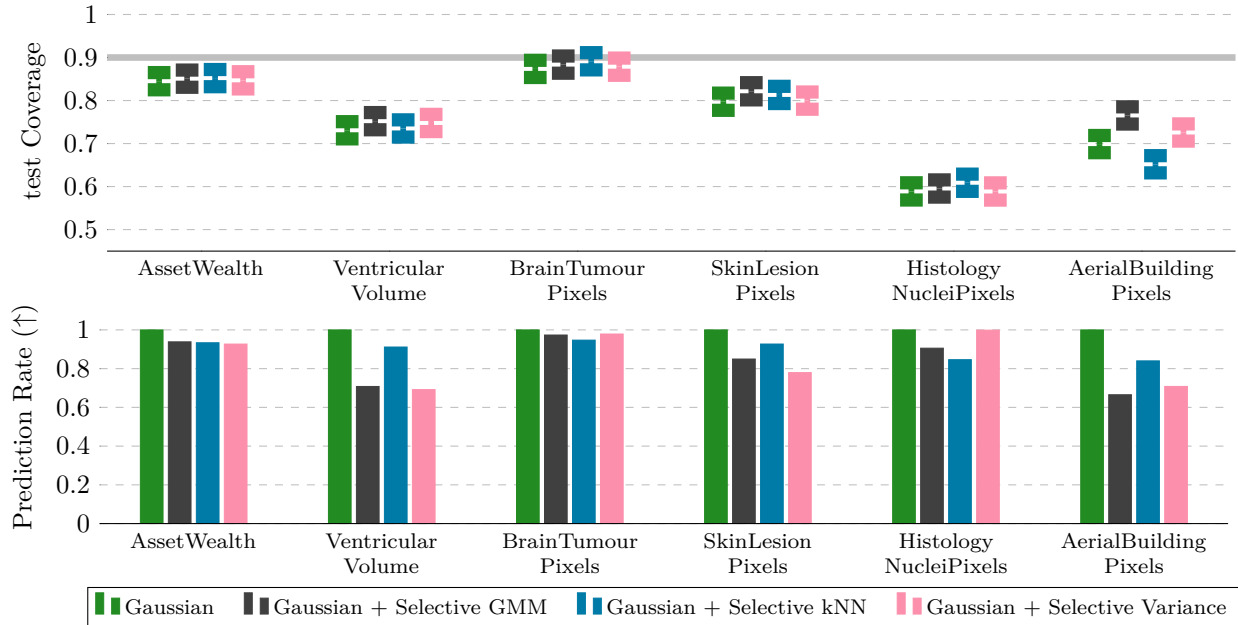


Figure 5: Results for the selective prediction methods based on GAUSSIAN, on the real-world datasets.

explanation is that real-world data requires better models for $p(x)$, i.e. that the relatively simple approaches based on feature-space density not are sufficient.

OOD Uncertainty Scores Perform Well, but Not Well Enough Comparing the selective prediction methods, we observe that GAUSSIAN + SELECTIVE GMM consistently outperforms GAUSSIAN + SELECTIVE VARIANCE (Figure 4 & 5) and that GAUSSIAN ENSEMBLE + SELECTIVE GMM outperforms GAUSSIAN ENSEMBLE + SELECTIVE ENSEMBLE VARIANCE in most cases (Figure A1 & A2). Relative to common uncertainty estimation baselines, methods based on feature-space density thus achieve very strong performance. This is in line with the state-of-the-art OOD detection performance that has been demonstrated recently. In our results, we can however clearly observe that while feature-space methods perform well *relative* to common baselines, the resulting selective prediction methods are still overconfident in many cases – the *absolute* performance is still far from perfect. Using our benchmark, we are thus able to not only compare the relative performance of different OOD uncertainty scores, but also evaluate their performance in an absolute sense.

Performance Differences among Real-World Datasets are Mostly Logical When we compare the performance on the different real-world datasets in Figure 3, all methods are relatively well-calibrated on BRAINTUMOURPIXELS and ASSETWEALTH. For BRAINTUMOURPIXELS, the train, val and test splits were created by randomly splitting the original set of MRI scans. The distribution shift between train/val and test is thus also fairly limited. For ASSETWEALTH (satellite images from different African countries), the shift is likely quite limited at least compared to AERIALBUILDINGPIXELS (satellite images from two different continents). Finally, the results for HISTOLOGYNUCLEIPIXELS are interesting, as this is the only dataset where CONFORMAL PREDICTION clearly obtains the best test coverage. It is not clear why the methods which output prediction intervals of input-dependent length struggle on this particular dataset.

7 Conclusion

We proposed an extensive benchmark for testing the reliability of regression uncertainty estimation methods under real-world distribution shifts. The benchmark consists of 8 publicly available image-based regression datasets with different types of challenging distribution shifts. We employed our benchmark to evaluate many of the most common uncertainty estimation methods, as well as two state-of-the-art uncertainty scores from OOD detection. We found that while all methods are well calibrated when there is no distribution shift, they

become highly overconfident on many of the benchmark datasets. Methods based on the OOD uncertainty scores performed well relative to other methods, but the absolute performance is still far from perfect. This uncovers important limitations of current regression uncertainty estimation methods. Our work thus serves as a challenge to the research community, to develop methods which actually produce calibrated prediction intervals across all benchmark datasets. To that end, future directions include exploring the use of more sophisticated models for $p(x)$ within selective prediction – hopefully closing the performance gap between synthetic and real-world datasets – and employing alternative DNN backbone architectures. We hope that our benchmark will spur more work on how to develop truly reliable regression uncertainty estimation methods.

Acknowledgements

This research was supported by the Swedish Research Council via the projects *NewLEADS – New Directions in Learning Dynamical Systems* (contract number: 621-2016-06079) and *Deep Probabilistic Regression – New Models and Learning Algorithms* (contract number: 2021-04301), and by the *Kjell & Märta Beijer Foundation*.

References

Michela Antonelli, Annika Reinke, Spyridon Bakas, Keyvan Farahani, Annette Kopp-Schneider, Bennett A Landman, Geert Litjens, Bjoern Menze, Olaf Ronneberger, Ronald M Summers, et al. The medical segmentation decathlon. *Nature Communications*, 13(1):1–13, 2022.

Spyridon Bakas, Hamed Akbari, Aristeidis Sotiras, Michel Bilello, Martin Rozycki, Justin S Kirby, John B Freymann, Keyvan Farahani, and Christos Davatzikos. Advancing the cancer genome atlas glioma mri collections with expert segmentation labels and radiomic features. *Scientific data*, 4(1):1–13, 2017.

Spyridon Bakas, Mauricio Reyes, Andras Jakab, Stefan Bauer, Markus Rempfler, Alessandro Crimi, Russell Takeshi Shinohara, Christoph Berger, Sung Min Ha, Martin Rozycki, et al. Identifying the best machine learning algorithms for brain tumor segmentation, progression assessment, and overall survival prediction in the brats challenge. *arXiv preprint arXiv:1811.02629*, 2018.

Charles Blundell, Julien Cornebise, Koray Kavukcuoglu, and Daan Wierstra. Weight uncertainty in neural network. In *International Conference on Machine Learning (ICML)*, pp. 1613–1622, 2015.

Kurtland Chua, Roberto Calandra, Rowan McAllister, and Sergey Levine. Deep reinforcement learning in a handful of trials using probabilistic dynamics models. In *Advances in Neural Information Processing Systems (NeurIPS)*, pp. 4759–4770, 2018.

Youngseog Chung, Willie Neiswanger, Ian Char, and Jeff Schneider. Beyond pinball loss: Quantile methods for calibrated uncertainty quantification. *Advances in Neural Information Processing Systems (NeurIPS)*, 34:10971–10984, 2021.

James H Cole, Rudra PK Poudel, Dimosthenis Tsagkrasoulis, Matthan WA Caan, Claire Steves, Tim D Spector, and Giovanni Montana. Predicting brain age with deep learning from raw imaging data results in a reliable and heritable biomarker. *NeuroImage*, 163:115–124, 2017.

Peng Cui, Wenbo Hu, and Jun Zhu. Calibrated reliable regression using maximum mean discrepancy. *Advances in Neural Information Processing Systems (NeurIPS)*, 33:17164–17175, 2020.

Xin Ding, Yongwei Wang, Zuheng Xu, William J. Welch, and Z. Jane Wang. Continuous conditional generative adversarial networks for image generation: Novel losses and label input mechanisms. *arXiv preprint arXiv:2011.07466*, 2020.

Xin Ding, Yongwei Wang, Zuheng Xu, William J Welch, and Z. Jane Wang. CcGAN: Continuous conditional generative adversarial networks for image generation. In *International Conference on Learning Representations (ICLR)*, 2021.

Samuel G Finlayson, Adarsh Subbaswamy, Karandeep Singh, John Bowers, Annabel Kupke, Jonathan Zittrain, Isaac S Kohane, and Suchi Saria. The clinician and dataset shift in artificial intelligence. *New England Journal of Medicine*, 385(3):283–286, 2021.

Yarin Gal. *Uncertainty in Deep Learning*. PhD thesis, University of Cambridge, 2016.

Yarin Gal and Zoubin Ghahramani. Dropout as a Bayesian approximation: Representing model uncertainty in deep learning. In *International Conference on Machine Learning (ICML)*, pp. 1050–1059, 2016.

Yonatan Geifman and Ran El-Yaniv. Selective classification for deep neural networks. *Advances in Neural Information Processing Systems (NeurIPS)*, 30, 2017.

Tilmann Gneiting, Fadoua Balabdaoui, and Adrian E Raftery. Probabilistic forecasts, calibration and sharpness. *Journal of the Royal Statistical Society: Series B (Statistical Methodology)*, 69(2):243–268, 2007.

Simon Graham, Quoc Dang Vu, Shan E Ahmed Raza, Ayesha Azam, Yee Wah Tsang, Jin Tae Kwak, and Nasir Rajpoot. HoVer-Net: Simultaneous segmentation and classification of nuclei in multi-tissue histology images. *Medical Image Analysis*, 58:101563, 2019.

Chuan Guo, Geoff Pleiss, Yu Sun, and Kilian Q Weinberger. On calibration of modern neural networks. In *Proceedings of the 34th International Conference on Machine Learning (ICML)*, pp. 1321–1330, 2017.

Fredrik K Gustafsson, Martin Danelljan, Goutam Bhat, and Thomas B Schön. Energy-based models for deep probabilistic regression. In *Proceedings of the European Conference on Computer Vision (ECCV)*, pp. 325–343, 2020a.

Fredrik K Gustafsson, Martin Danelljan, and Thomas B Schön. Evaluating scalable Bayesian deep learning methods for robust computer vision. In *Proceedings of the IEEE/CVF Conference on Computer Vision and Pattern Recognition (CVPR) Workshops*, 2020b.

Kaiming He, Xiangyu Zhang, Shaoqing Ren, and Jian Sun. Deep residual learning for image recognition. In *Proceedings of the IEEE Conference on Computer Vision and Pattern Recognition (CVPR)*, pp. 770–778, 2016.

Dan Hendrycks and Thomas Dietterich. Benchmarking neural network robustness to common corruptions and perturbations. In *International Conference on Learning Representations (ICLR)*, 2019.

Dan Hendrycks, Steven Basart, Norman Mu, Saurav Kadavath, Frank Wang, Evan Dorundo, Rahul Desai, Tyler Zhu, Samyak Parajuli, Mike Guo, et al. The many faces of robustness: A critical analysis of out-of-distribution generalization. In *Proceedings of the IEEE/CVF International Conference on Computer Vision (ICCV)*, pp. 8340–8349, 2021a.

Dan Hendrycks, Kevin Zhao, Steven Basart, Jacob Steinhardt, and Dawn Song. Natural adversarial examples. In *Proceedings of the IEEE/CVF Conference on Computer Vision and Pattern Recognition (CVPR)*, pp. 15262–15271, 2021b.

Dan Hendrycks, Andy Zou, Mantas Mazeika, Leonard Tang, Bo Li, Dawn Song, and Jacob Steinhardt. Pixmix: Dreamlike pictures comprehensively improve safety measures. In *Proceedings of the IEEE/CVF Conference on Computer Vision and Pattern Recognition (CVPR)*, pp. 16783–16792, 2022.

Radu Herbei and Marten H Wegkamp. Classification with reject option. *The Canadian Journal of Statistics/La Revue Canadienne de Statistique*, pp. 709–721, 2006.

Eddy Ilg, Ozgun Cicek, Silvio Galessio, Aaron Klein, Osama Makansi, Frank Hutter, and Thomas Bro. Uncertainty estimates and multi-hypotheses networks for optical flow. In *Proceedings of the European Conference on Computer Vision (ECCV)*, pp. 652–667, 2018.

Pavel Izmailov, Patrick Nicholson, Sanae Lotfi, and Andrew G Wilson. Dangers of bayesian model averaging under covariate shift. *Advances in Neural Information Processing Systems (NeurIPS)*, 34:3309–3322, 2021.

Vilde Jensen, Filippo Maria Bianchi, and Stian Norman Anfinsen. Ensemble conformalized quantile regression for probabilistic time series forecasting. *arXiv preprint arXiv:2202.08756*, 2022.

Wenming Jiang, Ying Zhao, and Zehan Wang. Risk-controlled selective prediction for regression deep neural network models. In *2020 International Joint Conference on Neural Networks (IJCNN)*, pp. 1–8. IEEE, 2020.

Benedikt Atli Jónsson, Gyda Björnsdóttir, TE Thorgeirsson, Lotta María Ellingsen, G Bragi Walters, DF Gudbjartsson, Hreinn Stefansson, Kari Stefansson, and MO Ulfarsson. Brain age prediction using deep learning uncovers associated sequence variants. *Nature Communications*, 10(1):5409, 2019.

Alex Kendall and Yarin Gal. What uncertainties do we need in Bayesian deep learning for computer vision? In *Advances in Neural Information Processing Systems (NeurIPS)*, pp. 5574–5584, 2017.

Diederik P Kingma and Jimmy Ba. Adam: A method for stochastic optimization. *arXiv preprint arXiv:1412.6980*, 2014.

Roger Koenker and Gilbert Bassett Jr. Regression quantiles. *Econometrica: journal of the Econometric Society*, pp. 33–50, 1978.

Pang Wei Koh, Shiori Sagawa, Henrik Marklund, Sang Michael Xie, Marvin Zhang, Akshay Balsubramani, Weihua Hu, Michihiro Yasunaga, Richard Lanas Phillips, Irena Gao, et al. Wilds: A benchmark of in-the-wild distribution shifts. In *International Conference on Machine Learning (ICML)*, pp. 5637–5664. PMLR, 2021.

Johnson Kuan and Jonas Mueller. Back to the basics: Revisiting out-of-distribution detection baselines. *arXiv preprint arXiv:2207.03061*, 2022.

Volodymyr Kuleshov, Nathan Fenner, and Stefano Ermon. Accurate uncertainties for deep learning using calibrated regression. In *International Conference on Machine Learning (ICML)*, pp. 2796–2804. PMLR, 2018.

Neeraj Kumar, Ruchiika Verma, Sanuj Sharma, Surabhi Bhargava, Abhishek Vahadane, and Amit Sethi. A dataset and a technique for generalized nuclear segmentation for computational pathology. *IEEE Transactions on Medical Imaging*, 36(7):1550–1560, 2017.

Balaji Lakshminarayanan, Alexander Pritzel, and Charles Blundell. Simple and scalable predictive uncertainty estimation using deep ensembles. In *Advances in Neural Information Processing Systems (NeurIPS)*, pp. 6402–6413, 2017.

Taro Langner, Robin Strand, Håkan Ahlström, and Joel Kullberg. Large-scale biometry with interpretable neural network regression on uk biobank body mri. *Scientific Reports*, 10(1):17752, 2020.

Taro Langner, Fredrik K Gustafsson, Benny Avelin, Robin Strand, Håkan Ahlström, and Joel Kullberg. Uncertainty-aware body composition analysis with deep regression ensembles on uk biobank mri. *Computerized Medical Imaging and Graphics*, 93:101994, 2021.

Stéphane Lathuilière, Pablo Mesejo, Xavier Alameda-Pineda, and Radu Horaud. A comprehensive analysis of deep regression. *IEEE Transactions on Pattern Analysis and Machine Intelligence (TPAMI)*, 2019.

Hei Law and Jia Deng. Cornernet: Detecting objects as paired keypoints. In *Proceedings of the European Conference on Computer Vision (ECCV)*, pp. 734–750, 2018.

Dan Levi, Liran Gispan, Niv Giladi, and Ethan Fetaya. Evaluating and calibrating uncertainty prediction in regression tasks. *Sensors*, 22(15):5540, 2022.

Yi-An Ma, Tianqi Chen, and Emily Fox. A complete recipe for stochastic gradient MCMC. In *Advances in Neural Information Processing Systems (NeurIPS)*, pp. 2917–2925, 2015.

Emmanuel Maggiori, Yuliya Tarabalka, Guillaume Charpiat, and Pierre Alliez. Can semantic labeling methods generalize to any city? the Inria aerial image labeling benchmark. In *2017 IEEE International Geoscience and Remote Sensing Symposium (IGARSS)*, pp. 3226–3229. IEEE, 2017.

Andrey Malinin, Neil Band, Yarin Gal, Mark Gales, Alexander Ganshin, German Chesnokov, Alexey Noskov, Andrey Ploskonosov, Liudmila Prokhorenkova, Ivan Prosvirkov, Vatsal Raina, Vyas Raina, Denis Roginskiy, Mariya Shmatova, Panagiotis Tigas, and Boris Yangel. Shifts: A dataset of real distributional shift across multiple large-scale tasks. In *Thirty-fifth Conference on Neural Information Processing Systems (NeurIPS), Datasets and Benchmarks Track*, 2021.

Bjoern H Menze, Andras Jakab, Stefan Bauer, Jayashree Kalpathy-Cramer, Keyvan Farahani, Justin Kirby, Yuliya Burren, Nicole Porz, Johannes Slotboom, Roland Wiest, et al. The multimodal brain tumor image segmentation benchmark (BRATS). *IEEE Transactions on Medical Imaging*, 34(10):1993–2024, 2014.

Takeru Miyato, Toshiki Kataoka, Masanori Koyama, and Yuichi Yoshida. Spectral normalization for generative adversarial networks. In *International Conference on Learning Representations (ICLR)*, 2018.

Jishnu Mukhoti, Andreas Kirsch, Joost van Amersfoort, Philip HS Torr, and Yarin Gal. Deep deterministic uncertainty: A simple baseline. *arXiv preprint*, 2021a.

Jishnu Mukhoti, Andreas Kirsch, Joost van Amersfoort, Philip HS Torr, and Yarin Gal. Deterministic neural networks with appropriate inductive biases capture epistemic and aleatoric uncertainty. *arXiv preprint arXiv:2102.11582*, 2021b.

Peter Naylor, Marick Laé, Fabien Reyal, and Thomas Walter. Segmentation of nuclei in histopathology images by deep regression of the distance map. *IEEE Transactions on Medical Imaging*, 38(2):448–459, 2018.

Radford M Neal. *Bayesian learning for neural networks*. PhD thesis, University of Toronto, 1995.

David Ouyang, Bryan He, Amirata Ghorbani, Neal Yuan, Joseph Ebinger, Curtis P Langlotz, Paul A Heidenreich, Robert A Harrington, David H Liang, Euan A Ashley, et al. Video-based AI for beat-to-beat assessment of cardiac function. *Nature*, 580(7802):252–256, 2020.

Yaniv Ovadia, Emily Fertig, Jie Ren, Zachary Nado, D. Sculley, Sebastian Nowozin, Joshua Dillon, Balaji Lakshminarayanan, and Jasper Snoek. Can you trust your model's uncertainty? Evaluating predictive uncertainty under dataset shift. In *Advances in Neural Information Processing Systems (NeurIPS)*, volume 32, 2019.

Harris Papadopoulos. Inductive conformal prediction: Theory and application to neural networks. In *Tools in artificial intelligence*. Citeseer, 2008.

Harris Papadopoulos, Kostas Proedrou, Volodya Vovk, and Alex Gammerman. Inductive confidence machines for regression. In *European Conference on Machine Learning*, pp. 345–356. Springer, 2002.

Adam Paszke, Sam Gross, Francisco Massa, Adam Lerer, James Bradbury, Gregory Chanan, Trevor Killeen, Zeming Lin, Natalia Gimelshein, Luca Antiga, et al. PyTorch: An imperative style, high-performance deep learning library. In *Advances in Neural Information Processing Systems (NeurIPS)*, pp. 8024–8035, 2019.

Fabian Pedregosa, Gaël Varoquaux, Alexandre Gramfort, Vincent Michel, Bertrand Thirion, Olivier Grisel, Mathieu Blondel, Peter Prettenhofer, Ron Weiss, Vincent Dubourg, Jake Vanderplas, Alexandre Passos, David Cournapeau, Matthieu Brucher, Matthieu Perrot, and Édouard Duchesnay. Scikit-learn: Machine learning in python. *Journal of Machine Learning Research (JMLR)*, 12(85):2825–2830, 2011.

Ethan Pickering and Themistoklis P Sapsis. Structure and distribution metric for quantifying the quality of uncertainty: Assessing gaussian processes, deep neural nets, and deep neural operators for regression. *arXiv preprint arXiv:2203.04515*, 2022.

Geoff Pleiss, Amauri Souza, Joseph Kim, Boyi Li, and Kilian Q. Weinberger. Neural network out-of-distribution detection for regression tasks, 2020. URL <https://openreview.net/forum?id=ryxsUySFwr>.

Ryan Poplin, Avinash V Varadarajan, Katy Blumer, Yun Liu, Michael V McConnell, Greg S Corrado, Lily Peng, and Dale R Webster. Prediction of cardiovascular risk factors from retinal fundus photographs via deep learning. *Nature Biomedical Engineering*, 2(3):158–164, 2018.

Joaquin Quionero-Candela, Masashi Sugiyama, Anton Schwaighofer, and Neil D Lawrence. Dataset shift in machine learning, 2009.

Yaniv Romano, Evan Patterson, and Emmanuel Candes. Conformalized quantile regression. *Advances in Neural Information Processing Systems (NeurIPS)*, 32, 2019.

Rasmus Rothe, Radu Timofte, and Luc Van Gool. Deep expectation of real and apparent age from a single image without facial landmarks. *International Journal of Computer Vision*, 126(2-4):144–157, 2016.

Mohammadreza Salehi, Hossein Mirzaei, Dan Hendrycks, Yixuan Li, Mohammad Hossein Rohban, and Mohammad Sabokrou. A unified survey on anomaly, novelty, open-set, and out-of-distribution detection: Solutions and future challenges. *Transactions on Machine Learning Research (TMLR)*, 2022.

Leo Schwinn, Leon Bungert, An Nguyen, René Raab, Falk Pulsmeyer, Doina Precup, Björn Eskofier, and Dario Zanca. Improving robustness against real-world and worst-case distribution shifts through decision region quantification. In *International Conference on Machine Learning (ICML)*, pp. 19434–19449. PMLR, 2022.

Joan Serrà, David Álvarez, Vicenç Gómez, Olga Slizovskaia, José F. Núñez, and Jordi Luque. Input complexity and out-of-distribution detection with likelihood-based generative models. In *International Conference on Learning Representations (ICLR)*, 2020.

Shaoshuai Shi, Xiaogang Wang, and Hongsheng Li. PointRCNN: 3d object proposal generation and detection from point cloud. In *Proceedings of the IEEE Conference on Computer Vision and Pattern Recognition (CVPR)*, pp. 770–779, 2019.

Wen Shi, Guohui Yan, Yamin Li, Haotian Li, Tingting Liu, Cong Sun, Guangbin Wang, Yi Zhang, Yu Zou, and Dan Wu. Fetal brain age estimation and anomaly detection using attention-based deep ensembles with uncertainty. *NeuroImage*, 223:117316, 2020.

Amber L Simpson, Michela Antonelli, Spyridon Bakas, Michel Bilello, Keyvan Farahani, Bram Van Ginneken, Annette Kopp-Schneider, Bennett A Landman, Geert Litjens, Bjoern Menze, et al. A large annotated medical image dataset for the development and evaluation of segmentation algorithms. *arXiv preprint arXiv:1902.09063*, 2019.

Ingo Steinwart and Andreas Christmann. Estimating conditional quantiles with the help of the pinball loss. *Bernoulli*, 17(1):211–225, 2011.

Yiyou Sun, Yifei Ming, Xiaojin Zhu, and Yixuan Li. Out-of-distribution detection with deep nearest neighbors. In *International Conference on Machine Learning (ICML)*, 2022.

Eric J Topol. High-performance medicine: the convergence of human and artificial intelligence. *Nature Medicine*, 25(1):44–56, 2019.

Philipp Tschandl, Cliff Rosendahl, and Harald Kittler. The HAM10000 dataset, a large collection of multi-source dermatoscopic images of common pigmented skin lesions. *Scientific data*, 5(1):1–9, 2018.

Olivia Wiles, Sven Gowal, Florian Stimberg, Sylvestre-Alvise Rebuffi, Ira Ktena, Krishnamurthy Dj Dvijotham, and Ali Taylan Cemgil. A fine-grained analysis on distribution shift. In *International Conference on Learning Representations (ICLR)*, 2022.

Bin Xiao, Haiping Wu, and Yichen Wei. Simple baselines for human pose estimation and tracking. In *Proceedings of the European Conference on Computer Vision (ECCV)*, pp. 466–481, 2018.

Wufeng Xue, Ali Islam, Mousumi Bhaduri, and Shuo Li. Direct multitype cardiac indices estimation via joint representation and regression learning. *IEEE Transactions on Medical Imaging*, 36(10):2057–2067, 2017.

Huaxiu Yao, Yu Wang, Sai Li, Linjun Zhang, Weixin Liang, James Zou, and Chelsea Finn. Improving out-of-distribution robustness via selective augmentation. In *International Conference on Machine Learning (ICML)*, pp. 25407–25437. PMLR, 2022.

Christopher Yeh, Anthony Perez, Anne Driscoll, George Azzari, Zhongyi Tang, David Lobell, Stefano Ermon, and Marshall Burke. Using publicly available satellite imagery and deep learning to understand economic well-being in Africa. *Nature communications*, 11(1):1–11, 2020.

Sheheryar Zaidi, Arber Zela, Thomas Elsken, Chris C Holmes, Frank Hutter, and Yee Teh. Neural ensemble search for uncertainty estimation and dataset shift. *Advances in Neural Information Processing Systems (NeurIPS)*, 34:7898–7911, 2021.

Marvin Mengxin Zhang, Sergey Levine, and Chelsea Finn. MEMO: Test time robustness via adaptation and augmentation. In *Advances in Neural Information Processing Systems (NeurIPS)*, 2022.

Zheng Zhu, Qiang Wang, Bo Li, Wei Wu, Junjie Yan, and Weiming Hu. Distractor-aware siamese networks for visual object tracking. In *Proceedings of the European Conference on Computer Vision (ECCV)*, pp. 101–117, 2018.

A Dataset Details

More detailed descriptions of the 12 datasets from Section 3.1 are provided below.

Cells Given a synthetic fluorescence microscopy image x , the task is to predict the number of cells y in the image. We utilize the Cell-200 dataset from Ding et al. (2021; 2020), consisting of 200 000 grayscale images of size 64×64 . We randomly draw 10 000 train images, 2 000 val images and 10 000 test images. Thus, there is no distribution shift between train/val and test. We therefore use this as a baseline dataset.

Cells-Tails We create a variant of CELLS with a clear distribution shift between train/val and test. For the 10 000 train images and 2 000 val images, the regression targets y are limited to the range $]50, 150]$. For the 10 000 test images, the targets instead lie in the full original range $[1, 200]$.

Cells-Gap Another variant of CELLS with a clear distribution shift between train/val and test. For the 10 000 train images and 2 000 val images, the regression targets y are limited to $[1, 50] \cup [150, 200]$. For the 10 000 test images, the targets instead lie in the full original range $[1, 200]$.

ChairAngle Given a synthetic image x of a rendered chair model, the task is to predict the yaw angle y of the chair. We utilize the RC-49 dataset from Ding et al. (2021; 2020), which contains 64×64 RGB images of different chair models rendered at 899 yaw angles ranging from 0.1° to 89.9° , with step size 0.1° . We randomly split their training set and obtain 17 640 train images and 4 410 val images. By sub-sampling their test set we also get 11 225 test images. There is no obvious distribution shift between train/val and test, and we therefore use this as a second baseline dataset.

ChairAngle-Tails We create a variant of CHAIRANGLE with a clear distribution shift between train/val and test. For train and val, we limit the regression targets y to the range $]15, 75[$. For test, the targets instead lie in the full original range $]0, 90[$. We obtain 11 760 train images, 2 940 val images and 11 225 test images.

ChairAngle-Gap Another variant of CHAIRANGLE with a clear distribution shift between train/val and test. For the 11 760 train images and 2 940 val images, the regression targets y are limited to $]0, 30] \cup [60, 90[$. For the 11 225 test images, the targets instead lie in the full original range $]0, 90[$.

AssetWealth Given a satellite image x (8 image channels), the task is to predict the asset wealth index y of the region. We utilize the PovertyMap-Wilds dataset (Koh et al., 2021), which is a variant of the dataset collected by Yeh et al. (2020). We use the training, validation-ID and test-OOD subsets of the data, giving us 9 797 train images, 1 000 val images and 3 963 test images. We resize the images from size 224×224 to 64×64 . Train/val and test contain satellite images from disjoint sets of African countries, creating a distribution shift.

VentricularVolume Given an echocardiogram image x of a human heart, the task is to predict the volume y of the left ventricle. We utilize the EchoNet-Dynamic dataset by Ouyang et al. (2020), which contains 10 030 echocardiogram videos. Each video captures a complete cardiac cycle and is labeled with measurements of the left ventricular volume at two separate time points, representing end-systole (at the end of contraction - smaller volume) and end-diastole (just before contraction - larger volume). For each video, we extract just one of these volume measurements along with the corresponding video frame. To create a clear distribution shift between train/val and test, we select the end systolic volume (smaller volume) for train and val, but the end diastolic volume (larger volume) for test. We utilize the provided dataset splits, giving us 7 460 train images, 1 288 val images and 1 276 test images. We resize the images from size 112×112 to 64×64 .

BrainTumourPixels Given an image slice x of a brain MRI scan, the task is to predict the number of pixels y in the image which are labeled as brain tumour. We utilize the brain tumour dataset of the medical segmentation decathlon (Simpson et al., 2019; Antonelli et al., 2022), which is a subset of the data used in the 2016 and 2017 BraTS challenges (Bakas et al., 2018; 2017; Menze et al., 2014). The dataset contains 484 brain MRI scans with corresponding tumour segmentation masks. We split these scans 80%/20%/20% into train, val and test sets. The scans are 3D volumes of size $240 \times 240 \times 155$. We convert each scan into 155 image slices of size 240×240 , and create a regression target for each image by counting the number of labeled brain tumour pixels. We then also remove all images which contain no tumour pixels. The original image slices have 4 channels (FLAIR, T1w, T1gd, T2w), but we only use the first three and convert the slices into standard RGB images. This gives us 20 614 train images, 6 116 val images and 6 252 test images. We also resize the images from size 240×240 to 64×64 .

SkinLesionPixels Given a dermatoscopic image x of a pigmented skin lesion, the task is to predict the number of pixels y in the image which are labeled as lesion. We utilize the HAM10000 dataset by Tschandl et al. (2018), which contains 10 015 dermatoscopic images with corresponding skin lesion segmentation masks. HAM10000 consists of four different sub-datasets, three of which (ViDIR Legacy, ViDIR Current and ViDIR MoleMax) were collected in Austria, while the fourth sub-dataset (Rosendahl) was collected in Australia. To create a clear distribution shift between train/val and test, we use the Australian sub-dataset (Rosendahl) as our test set. After randomly splitting the remaining images 85%/15% into train and val sets, we obtain 6 592 train images, 1 164 val images and 2 259 test images. We then create a regression target for each image by counting the number of labeled skin lesion pixels. We also resize the images from size 450×600 to 64×64 .

HistologyNucleiPixels Given an H&E stained histology image x , the task is to predict the number of pixels y in the image which are labeled as nuclei. We utilize the CoNSeP dataset by Graham et al. (2019), along with the pre-processed versions they provide of the Kumar (Kumar et al., 2017) and TNBC (Naylor et al., 2018) datasets. The datasets contain large H&E stained image tiles (of size 1000×1000 or 512×512) at $40\times$ objective magnification, with corresponding nuclear segmentation masks. The three datasets were collected at different hospitals/institutions, with differing procedures for specimen preservation and staining. By using CoNSeP and Kumar for train/val and TNBC for test, we thus obtain a clear distribution shift. From the large image tiles, we extract 64×64 patches via regular gridding, and create a regression target for each image patch by counting the number of labeled nuclei pixels. We then also remove all images which contain no nuclei pixels. In the end, we obtain 10 808 train images, 2 702 val images and 2 267 test images.

AerialBuildingPixels Given an aerial image x , the task is to predict the number of pixels y in the image which are labeled as building. We utilize the Inria aerial image labeling dataset (Maggiori et al., 2017), which contains 180 large aerial images with corresponding building segmentation masks. The images are of size 5000×5000 , and are captured at five different geographical locations. We use the images from two densely populated American cities (Austin and Chicago) for train/val, and the images from a more rural European area (West Tyrol, Austria) for test, thus obtaining a clear distribution shift. We first resize the images to size 1000×1000 , and then extract 64×64 patches via regular gridding. We also create a regression target for each image patch by counting the number of labeled building pixels. After removal of all images which contain no building pixels, we finally obtain 11 184 train images, 2 797 val images and 3 890 test images.

B Additional Results & Method Variations

Please note that the results in Table A1 - Table A42 not are rounded/truncated to only significant digits.

To ensure that the test coverage results do not depend on our specific choice of studying 90% prediction intervals ($\alpha = 0.1$), we repeat most of the evaluation for two alternative miscoverage rates α . Specifically, we redo the evaluation of 6/10 methods on 9/12 datasets with 80% ($\alpha = 0.2$) and 95% ($\alpha = 0.05$) prediction intervals. The results for 80% prediction intervals are given in Table A13 - Table A21, and the results for 95% are given in Table A22 - Table A30. We observe very similar trends overall. For example, all methods still have almost perfectly calibrated prediction intervals on CELLS (Table A13 & A22) and CHAIRANGLE (Table A15 & A24), i.e. they all obtain a test coverage very close to 80%/95%, but only GAUSSIAN + SELECTIVE GMM remains well-calibrated on CELLS-TAILS and CHAIRANGLE-GAP. With the exception of BRAINTUMOURPIXELS, all methods are also significantly overconfident on all the real-world datasets.

Apart from the main comparison of the 10 methods specified in Section 4, we also evaluate a few method variations. The results for these experiments are provided in Table A31 - Table A42. For GAUSSIAN + SELECTIVE GMM, we vary the number of GMM mixture components from the standard $k = 4$ to $k = 2$ and $k = 8$, but observe no particularly consistent or significant trends in the results. Similarly, we vary the number of neighbors from the standard $k = 10$ to $k = 5$ and $k = 20$ for GAUSSIAN + SELECTIVE kNN, but observe no clear trends here either. For GAUSSIAN + SELECTIVE kNN, we also explore replacing the cosine similarity distance metric with L2 distance, again obtaining very similar results. Following Mukhoti et al. (2021b), we finally add spectral normalization (Miyato et al., 2018) for further feature-space regularization, but observe no significant improvements for GAUSSIAN + SELECTIVE GMM.

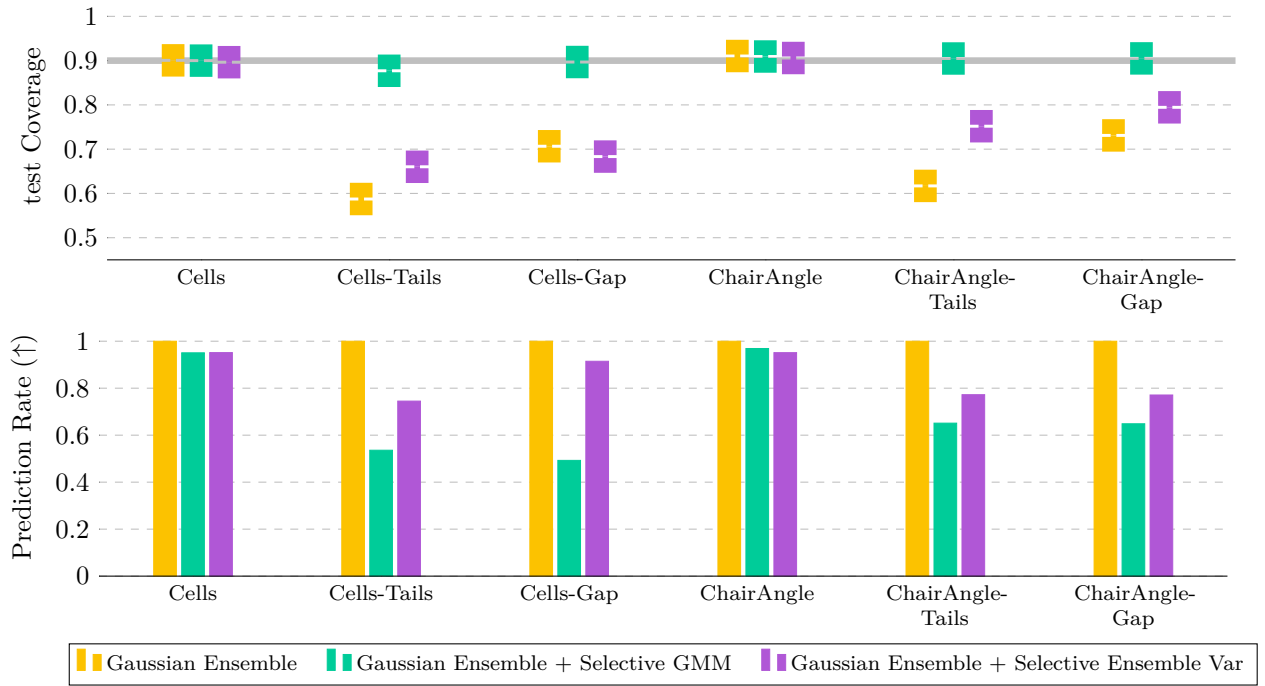


Figure A1: Results for selective prediction methods based on GAUSSIAN ENSEMBLE, on synthetic datasets.

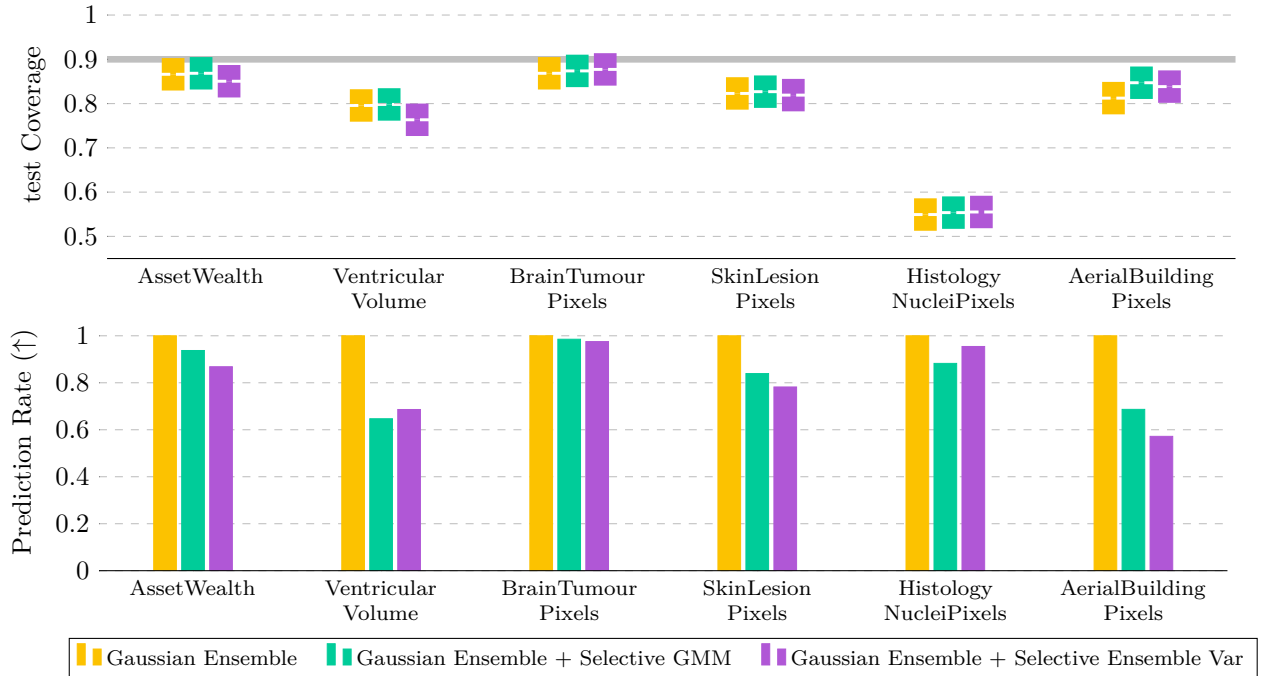


Figure A2: Results for selective prediction methods based on GAUSSIAN ENSEMBLE, on real-world datasets.

Table A1: Complete results on the CELLS dataset.

Method	val MAE (\downarrow)	val Interval Length (\downarrow)	test Coverage (≥ 0.90)	test Prediction Rate (\uparrow)
Conformal Prediction	4.03121 ± 2.78375	18.8216 ± 11.8302	0.9117 ± 0.00275173	1.0
Ensemble	2.22525 ± 0.471309	12.2881 ± 2.78795	0.8994 ± 0.00689986	1.0
Gaussian	3.61704 ± 1.13624	14.5492 ± 4.44927	0.90286 ± 0.00594629	1.0
Gaussian Ensemble	2.78757 ± 1.16951	17.1285 ± 4.33367	0.90062 ± 0.0027571	1.0
Quantile Regression	3.70405 ± 0.81647	13.8023 ± 2.19085	0.90486 ± 0.006771	1.0
Gaussian + Selective GMM	3.61704 ± 1.13624	14.5492 ± 4.44927	0.905241 ± 0.00448315	0.95216 ± 0.00290558
Gaussian + Selective kNN	3.61704 ± 1.13624	14.5492 ± 4.44927	0.900069 ± 0.00677637	0.94656 ± 0.00470472
Gaussian + Selective Variance	3.61704 ± 1.13624	14.5492 ± 4.44927	0.904839 ± 0.00795449	0.95712 ± 0.00200938
Gaussian Ensemble + Selective GMM	2.78757 ± 1.16951	17.1285 ± 4.33367	0.899999 ± 0.00311328	0.95066 ± 0.0023105
Gaussian Ensemble + Selective Ens Var	2.78757 ± 1.16951	17.1285 ± 4.33367	0.896465 ± 0.0015705	0.95156 ± 0.00215277

Table A2: Complete results on the CELLS-TAILS dataset.

Method	val MAE (\downarrow)	val Interval Length (\downarrow)	test Coverage (≥ 0.90)	test Prediction Rate (\uparrow)
Conformal Prediction	3.56733 ± 1.0818	14.2128 ± 4.23582	0.55356 ± 0.0299096	1.0
Ensemble	1.83461 ± 0.178937	9.8697 ± 1.6672	0.50078 ± 0.007608	1.0
Gaussian	4.05446 ± 1.33153	15.4321 ± 4.98796	0.54402 ± 0.0347525	1.0
Gaussian Ensemble	2.40691 ± 0.580524	10.9696 ± 1.70051	0.5874 ± 0.0479263	1.0
Quantile Regression	3.32571 ± 1.24578	13.0848 ± 3.54239	0.52222 ± 0.0284102	1.0
Gaussian + Selective GMM	4.05446 ± 1.33153	15.4321 ± 4.98796	0.889825 ± 0.0193021	0.53654 ± 0.0101012
Gaussian + Selective kNN	4.05446 ± 1.33153	15.4321 ± 4.98796	0.859179 ± 0.0255173	0.56692 ± 0.0127107
Gaussian + Selective Variance	4.05446 ± 1.33153	15.4321 ± 4.98796	0.687475 ± 0.0659807	0.6914 ± 0.0651196
Gaussian Ensemble + Selective GMM	2.40691 ± 0.580524	10.9696 ± 1.70051	0.877068 ± 0.0222502	0.53604 ± 0.0125903
Gaussian Ensemble + Selective Ens Var	2.40691 ± 0.580524	10.9696 ± 1.70051	0.660212 ± 0.0325832	0.74512 ± 0.0438128

Table A3: Complete results on the CELLS-GAP dataset.

Method	val MAE (\downarrow)	val Interval Length (\downarrow)	test Coverage (≥ 0.90)	test Prediction Rate (\uparrow)
Conformal Prediction	3.67702 ± 1.33587	17.1152 ± 6.49211	0.64002 ± 0.0620287	1.0
Ensemble	2.7261 ± 0.705274	13.4061 ± 2.40513	0.6771 ± 0.0544788	1.0
Gaussian	3.53089 ± 1.0619	15.6396 ± 6.23458	0.66028 ± 0.114703	1.0
Gaussian Ensemble	3.46118 ± 0.95429	18.707 ± 4.13287	0.7066 ± 0.0317638	1.0
Quantile Regression	4.75328 ± 1.73499	18.108 ± 4.21716	0.64488 ± 0.12875	1.0
Gaussian + Selective GMM	3.53089 ± 1.0619	15.6396 ± 6.23458	0.890569 ± 0.00953089	0.49372 ± 0.0025926
Gaussian + Selective kNN	3.53089 ± 1.0619	15.6396 ± 6.23458	0.874032 ± 0.0432364	0.53646 ± 0.0139864
Gaussian + Selective Variance	3.53089 ± 1.0619	15.6396 ± 6.23458	0.652766 ± 0.117192	0.9748 ± 0.000940213
Gaussian Ensemble + Selective GMM	3.46118 ± 0.95429	18.707 ± 4.13287	0.896848 ± 0.0127879	0.49278 ± 0.00192914
Gaussian Ensemble + Selective Ens Var	3.46118 ± 0.95429	18.707 ± 4.13287	0.68326 ± 0.0299799	0.9147 ± 0.0182427

Table A4: Complete results on the CHAIRANGLE dataset.

Method	val MAE (\downarrow)	val Interval Length (\downarrow)	test Coverage (≥ 0.90)	test Prediction Rate (\uparrow)
Conformal Prediction	0.289127 ± 0.081643	1.08752 ± 0.202247	0.905265 ± 0.00339915	1.0
Ensemble	0.189858 ± 0.0548452	0.788401 ± 0.137465	0.909915 ± 0.00399101	1.0
Gaussian	0.376692 ± 0.171928	1.37757 ± 0.382191	0.901577 ± 0.00308472	1.0
Gaussian Ensemble	0.361834 ± 0.165348	1.2044 ± 0.442422	0.910414 ± 0.00316257	1.0
Quantile Regression	0.851253 ± 0.544717	3.19741 ± 1.9751	0.906209 ± 0.00204038	1.0
Gaussian + Selective GMM	0.376692 ± 0.171928	1.37757 ± 0.382191	0.902482 ± 0.00436054	0.972739 ± 0.00191733
Gaussian + Selective kNN	0.376692 ± 0.171928	1.37757 ± 0.382191	0.90222 ± 0.00459694	0.975465 ± 0.00201785
Gaussian + Selective Variance	0.376692 ± 0.171928	1.37757 ± 0.382191	0.904805 ± 0.00765098	0.961782 ± 0.0193133
Gaussian Ensemble + Selective GMM	0.361834 ± 0.165348	1.2044 ± 0.442422	0.9093 ± 0.00297263	0.969033 ± 0.000940447
Gaussian Ensemble + Selective Ens Var	0.361834 ± 0.165348	1.2044 ± 0.442422	0.905905 ± 0.00336481	0.951359 ± 0.00453556

Table A5: Complete results on the CHAIRANGLE-TAILS dataset.

Method	val MAE (\downarrow)	val Interval Length (\downarrow)	test Coverage (≥ 0.90)	test Prediction Rate (\uparrow)
Conformal Prediction	0.358162 ± 0.168257	1.31102 ± 0.531401	0.615804 ± 0.00527695	1.0
Ensemble	0.21931 ± 0.0596705	1.04074 ± 0.245846	0.611706 ± 0.00345611	1.0
Gaussian	0.241214 ± 0.091736	1.09417 ± 0.382907	0.622592 ± 0.00714065	1.0
Gaussian Ensemble	0.13365 ± 0.0189933	0.769172 ± 0.0814039	0.617016 ± 0.0063698	1.0
Quantile Regression	0.820934 ± 0.653268	2.9815 ± 2.15473	0.660953 ± 0.0379624	1.0
Gaussian + Selective GMM	0.241214 ± 0.091736	1.09417 ± 0.382907	0.901946 ± 0.00382993	0.655448 ± 0.001058
Gaussian + Selective kNN	0.241214 ± 0.091736	1.09417 ± 0.382907	0.860311 ± 0.00617031	0.703038 ± 0.00691227
Gaussian + Selective Variance	0.241214 ± 0.091736	1.09417 ± 0.382907	0.647559 ± 0.0360179	0.924383 ± 0.0751205
Gaussian Ensemble + Selective GMM	0.13365 ± 0.0189933	0.769172 ± 0.0814039	0.904807 ± 0.00394199	0.651314 ± 0.0013893
Gaussian Ensemble + Selective Ens Var	0.13365 ± 0.0189933	0.769172 ± 0.0814039	0.751845 ± 0.0131765	0.772401 ± 0.00878839

Table A6: Complete results on the CHAIRANGLE-GAP dataset.

Method	val MAE (\downarrow)	val Interval Length (\downarrow)	test Coverage (≥ 0.90)	test Prediction Rate (\uparrow)
Conformal Prediction	0.35034 ± 0.161819	1.35 ± 0.547089	0.659546 ± 0.00916108	1.0
Ensemble	0.22898 ± 0.0853825	1.1222 ± 0.174147	0.749951 ± 0.0155327	1.0
Gaussian	0.454516 ± 0.280174	2.09212 ± 0.933756	0.69363 ± 0.0345876	1.0
Gaussian Ensemble	0.226352 ± 0.0677413	1.30588 ± 0.136235	0.731065 ± 0.0126216	1.0
Quantile Regression	0.639151 ± 0.296536	3.29137 ± 1.53269	0.695697 ± 0.0413613	1.0
Gaussian + Selective GMM	0.454516 ± 0.280174	2.09212 ± 0.933756	0.91215 ± 0.00604745	0.649372 ± 0.00334919
Gaussian + Selective kNN	0.454516 ± 0.280174	2.09212 ± 0.933756	0.911574 ± 0.00376608	0.673764 ± 0.0113432
Gaussian + Selective Variance	0.454516 ± 0.280174	2.09212 ± 0.933756	0.690436 ± 0.0366025	0.981292 ± 0.0152406
Gaussian Ensemble + Selective GMM	0.226352 ± 0.0677413	1.30588 ± 0.136235	0.905039 ± 0.00229837	0.648624 ± 0.00094348
Gaussian Ensemble + Selective Ens Var	0.226352 ± 0.0677413	1.30588 ± 0.136235	0.794531 ± 0.014876	0.7711 ± 0.0191172

Table A7: Complete results on the ASSETWEALTH dataset.

Method	val MAE (\downarrow)	val Interval Length (\downarrow)	test Coverage (≥ 0.90)	test Prediction Rate (\uparrow)
Conformal Prediction	0.346532 ± 0.00578306	1.5838 ± 0.0318086	0.87136 ± 0.0090944	1.0
Ensemble	0.320002 ± 0.00264202	1.45568 ± 0.0129312	0.87348 ± 0.00598963	1.0
Gaussian	0.367501 ± 0.0416437	1.597 ± 0.207599	0.844966 ± 0.0456831	1.0
Gaussian Ensemble	0.3295 ± 0.00783906	1.42071 ± 0.0485437	0.866162 ± 0.00711672	1.0
Quantile Regression	0.404279 ± 0.0683226	1.58957 ± 0.161689	0.823921 ± 0.0313343	1.0
Gaussian + Selective GMM	0.367501 ± 0.0416437	1.597 ± 0.207599	0.850824 ± 0.047533	0.93838 ± 0.0170443
Gaussian + Selective kNN	0.367501 ± 0.0416437	1.597 ± 0.207599	0.852107 ± 0.0474734	0.933586 ± 0.0203541
Gaussian + Selective Variance	0.367501 ± 0.0416437	1.597 ± 0.207599	0.846981 ± 0.0403247	0.926874 ± 0.0159098
Gaussian Ensemble + Selective GMM	0.3295 ± 0.00783906	1.42071 ± 0.0485437	0.868444 ± 0.00727312	0.937371 ± 0.0138213
Gaussian Ensemble + Selective Ens Var	0.3295 ± 0.00783906	1.42071 ± 0.0485437	0.85047 ± 0.00397082	0.868282 ± 0.0299149

Table A8: Complete results on the VENTRICULARVOLUME dataset.

Method	val MAE (\downarrow)	val Interval Length (\downarrow)	test Coverage (≥ 0.90)	test Prediction Rate (\uparrow)
Conformal Prediction	11.2471 ± 0.201399	47.4505 ± 1.556	0.603135 ± 0.0125842	1.0
Ensemble	10.2476 ± 0.113707	41.8445 ± 0.750822	0.707367 ± 0.00877743	1.0
Gaussian	12.7238 ± 1.52197	51.566 ± 3.52739	0.730878 ± 0.0619045	1.0
Gaussian Ensemble	10.1141 ± 0.180661	39.9817 ± 1.91308	0.795768 ± 0.0231243	1.0
Quantile Regression	12.4944 ± 0.676265	49.0448 ± 3.33314	0.710972 ± 0.045171	1.0
Gaussian + Selective GMM	12.7238 ± 1.52197	51.566 ± 3.52739	0.752046 ± 0.0529087	0.707994 ± 0.0208741
Gaussian + Selective kNN	12.7238 ± 1.52197	51.566 ± 3.52739	0.735105 ± 0.0612413	0.911599 ± 0.0447475
Gaussian + Selective Variance	12.7238 ± 1.52197	51.566 ± 3.52739	0.747868 ± 0.0569984	0.691693 ± 0.0341016
Gaussian Ensemble + Selective GMM	10.1141 ± 0.180661	39.9817 ± 1.91308	0.798094 ± 0.0166674	0.646865 ± 0.0366201
Gaussian Ensemble + Selective Ens Var	10.1141 ± 0.180661	39.9817 ± 1.91308	0.763412 ± 0.0286772	0.686207 ± 0.0431835

Table A9: Complete results on the BRAINTUMOURPIXELS dataset.

Method	val MAE (\downarrow)	val Interval Length (\downarrow)	test Coverage (≥ 0.90)	test Prediction Rate (\uparrow)
Conformal Prediction	21.3163 ± 0.45997	93.7169 ± 2.99061	0.885925 ± 0.00395743	1.0
Ensemble	21.1133 ± 0.210209	90.3825 ± 0.825858	0.878183 ± 0.00318872	1.0
Gaussian	21.0625 ± 0.358012	93.6284 ± 2.29916	0.873544 ± 0.00871896	1.0
Gaussian Ensemble	20.5336 ± 0.211421	87.7414 ± 0.818979	0.868426 ± 0.00328047	1.0
Quantile Regression	22.0348 ± 0.697606	94.3249 ± 3.07265	0.879079 ± 0.00380396	1.0
Gaussian + Selective GMM	21.0625 ± 0.358012	93.6284 ± 2.29916	0.883515 ± 0.0138279	0.973576 ± 0.0187252
Gaussian + Selective kNN	21.0625 ± 0.358012	93.6284 ± 2.29916	0.891264 ± 0.00734602	0.947185 ± 0.0178434
Gaussian + Selective Variance	21.0625 ± 0.358012	93.6284 ± 2.29916	0.878666 ± 0.00735197	0.978791 ± 0.00694672
Gaussian Ensemble + Selective GMM	20.5336 ± 0.211421	87.7414 ± 0.818979	0.873824 ± 0.00466519	0.985349 ± 0.00461984
Gaussian Ensemble + Selective Ens Var	20.5336 ± 0.211421	87.7414 ± 0.818979	0.877211 ± 0.00302057	0.975368 ± 0.00323397

Table A10: Complete results on the SKINLESIONPIXELS dataset.

Method	val MAE (\downarrow)	val Interval Length (\downarrow)	test Coverage (≥ 0.90)	test Prediction Rate (\uparrow)
Conformal Prediction	107.514 ± 1.87464	492.922 ± 14.1865	0.708012 ± 0.00917777	1.0
Ensemble	99.3156 ± 0.997867	353.842 ± 4.73577	0.742098 ± 0.00852236	1.0
Gaussian	105.417 ± 1.15178	535.139 ± 215.446	0.797255 ± 0.0270734	1.0
Gaussian Ensemble	100.639 ± 0.464183	472.14 ± 85.2654	0.822931 ± 0.0134328	1.0
Quantile Regression	113.076 ± 3.20875	405.904 ± 4.75158	0.719788 ± 0.0213826	1.0
Gaussian + Selective GMM	105.417 ± 1.15178	535.139 ± 215.446	0.821515 ± 0.0137705	0.849579 ± 0.0206181
Gaussian + Selective kNN	105.417 ± 1.15178	535.139 ± 215.446	0.813027 ± 0.0306586	0.927047 ± 0.00830718
Gaussian + Selective Variance	105.417 ± 1.15178	535.139 ± 215.446	0.799821 ± 0.0150855	0.77946 ± 0.059169
Gaussian Ensemble + Selective GMM	100.639 ± 0.464183	472.14 ± 85.2654	0.826921 ± 0.00719649	0.839132 ± 0.0108815
Gaussian Ensemble + Selective Ens Var	100.639 ± 0.464183	472.14 ± 85.2654	0.819129 ± 0.00910128	0.782116 ± 0.0109776

Table A11: Complete results on the HISTOLOGYNUCLEIPIXELS dataset.

Method	val MAE (\downarrow)	val Interval Length (\downarrow)	test Coverage (≥ 0.90)	test Prediction Rate (\uparrow)
Conformal Prediction	217.887 ± 3.71766	993.665 ± 18.3282	0.841288 ± 0.0128314	1.0
Ensemble	197.078 ± 1.99489	853.361 ± 14.1904	0.812704 ± 0.00664074	1.0
Gaussian	211.795 ± 10.0239	1211.83 ± 396.946	0.588796 ± 0.0912794	1.0
Gaussian Ensemble	196.785 ± 2.14454	1108.53 ± 145.034	0.54936 ± 0.05995	1.0
Quantile Regression	227.895 ± 9.37415	914.909 ± 45.995	0.684076 ± 0.0428704	1.0
Gaussian + Selective GMM	211.795 ± 10.0239	1211.83 ± 396.946	0.59554 ± 0.0956742	0.90569 ± 0.0453555
Gaussian + Selective kNN	211.795 ± 10.0239	1211.83 ± 396.946	0.608929 ± 0.0805954	0.846228 ± 0.0482832
Gaussian + Selective Variance	211.795 ± 10.0239	1211.83 ± 396.946	0.588598 ± 0.0913593	0.998765 ± 0.00134954
Gaussian Ensemble + Selective GMM	196.785 ± 2.14454	1108.53 ± 145.034	0.553725 ± 0.0642274	0.882488 ± 0.0156395
Gaussian Ensemble + Selective Ens Var	196.785 ± 2.14454	1108.53 ± 145.034	0.555149 ± 0.0620052	0.954477 ± 0.0256246

Table A12: Complete results on the AERIALBUILDINGPIXELS dataset.

Method	val MAE (\downarrow)	val Interval Length (\downarrow)	test Coverage (≥ 0.90)	test Prediction Rate (\uparrow)
Conformal Prediction	235.417 ± 7.16096	1038.45 ± 51.5565	0.637584 ± 0.0691102	1.0
Ensemble	199.206 ± 2.76543	798.312 ± 6.80986	0.772494 ± 0.0227288	1.0
Gaussian	217.877 ± 1.72493	929.562 ± 47.6606	0.698766 ± 0.0662263	1.0
Gaussian Ensemble	208.487 ± 1.03581	885.349 ± 27.8584	0.812339 ± 0.0617386	1.0
Quantile Regression	242.284 ± 6.0122	909.191 ± 24.9528	0.763342 ± 0.0902358	1.0
Gaussian + Selective GMM	217.877 ± 1.72493	929.562 ± 47.6606	0.76535 ± 0.0388677	0.652082 ± 0.0990489
Gaussian + Selective kNN	217.877 ± 1.72493	929.562 ± 47.6606	0.651867 ± 0.0771154	0.840103 ± 0.0463989
Gaussian + Selective Variance	217.877 ± 1.72493	929.562 ± 47.6606	0.725714 ± 0.0779575	0.708226 ± 0.103803
Gaussian Ensemble + Selective GMM	208.487 ± 1.03581	885.349 ± 27.8584	0.847101 ± 0.038266	0.686787 ± 0.0278702
Gaussian Ensemble + Selective Ens Var	208.487 ± 1.03581	885.349 ± 27.8584	0.838352 ± 0.0312236	0.571928 ± 0.0402727

Table A13: Miscoverage rate $\alpha = 0.2$: Results on the CELLS dataset.

Method	val MAE (\downarrow)	val Interval Length (\downarrow)	test Coverage (≥ 0.80)	test Prediction Rate (\uparrow)
Conformal Prediction	4.03121 ± 2.78375	14.042 ± 10.2791	0.811 ± 0.0100485	1.0
Gaussian	3.61704 ± 1.13624	11.544 ± 3.59513	0.808 ± 0.00859046	1.0
Gaussian Ensemble	2.78757 ± 1.16951	13.1298 ± 3.34997	0.80044 ± 0.00316582	1.0
Quantile Regression	4.40758 ± 1.47411	13.3314 ± 4.39511	0.80152 ± 0.00667005	1.0
Gaussian + Selective GMM	3.61704 ± 1.13624	11.544 ± 3.59513	0.811076 ± 0.00507358	0.95216 ± 0.00280043
Gaussian Ensemble + Selective Ens Var	2.78757 ± 1.16951	13.1298 ± 3.34997	0.793124 ± 0.00576659	0.95156 ± 0.00215277

Table A14: Miscoverage rate $\alpha = 0.2$: Results on the CELLS-TAILS dataset.

Method	val MAE (\downarrow)	val Interval Length (\downarrow)	test Coverage (≥ 0.80)	test Prediction Rate (\uparrow)
Conformal Prediction	3.56733 ± 1.0818	11.3841 ± 3.54242	0.48332 ± 0.0337429	1.0
Gaussian	4.05446 ± 1.33153	12.7086 ± 4.39552	0.47106 ± 0.0319074	1.0
Gaussian Ensemble	2.40691 ± 0.580524	8.62187 ± 1.5177	0.4768 ± 0.0461347	1.0
Quantile Regression	4.20398 ± 1.61554	13.1241 ± 4.61204	0.49358 ± 0.0341114	1.0
Gaussian + Selective GMM	4.05446 ± 1.33153	12.7086 ± 4.39552	0.788228 ± 0.0239896	0.5364 ± 0.0100584
Gaussian Ensemble + Selective Ens Var	2.40691 ± 0.580524	8.62187 ± 1.5177	0.567734 ± 0.0270648	0.74512 ± 0.0438128

Table A15: Miscoverage rate $\alpha = 0.2$: Results on the CHAIRANGLE dataset.

Method	val MAE (\downarrow)	val Interval Length (\downarrow)	test Coverage (≥ 0.80)	test Prediction Rate (\uparrow)
Conformal Prediction	0.289127 ± 0.081643	0.872808 ± 0.205426	0.80212 ± 0.00337798	1.0
Gaussian	0.376692 ± 0.171928	1.14193 ± 0.40832	0.806646 ± 0.00565869	1.0
Gaussian Ensemble	0.361834 ± 0.165348	1.01037 ± 0.399644	0.813452 ± 0.00329742	1.0
Quantile Regression	0.648062 ± 0.181932	1.87322 ± 0.428951	0.807127 ± 0.00380433	1.0
Gaussian + Selective GMM	0.376692 ± 0.171928	1.14193 ± 0.40832	0.807801 ± 0.0066405	0.972829 ± 0.0019256
Gaussian Ensemble + Selective Ens Var	0.361834 ± 0.165348	1.01037 ± 0.399644	0.804719 ± 0.00318856	0.951359 ± 0.00453556

Table A16: Miscoverage rate $\alpha = 0.2$: Results on the CHAIRANGLE-GAP dataset.

Method	val MAE (\downarrow)	val Interval Length (\downarrow)	test Coverage (≥ 0.80)	test Prediction Rate (\uparrow)
Conformal Prediction	0.35034 ± 0.161819	1.09877 ± 0.497591	0.588472 ± 0.0119766	1.0
Gaussian	0.454516 ± 0.280174	1.69802 ± 0.840083	0.613951 ± 0.0358797	1.0
Gaussian Ensemble	0.226352 ± 0.0677413	0.972076 ± 0.118477	0.6431 ± 0.0136145	1.0
Quantile Regression	0.692597 ± 0.269476	2.29958 ± 0.738934	0.600606 ± 0.0136385	1.0
Gaussian + Selective GMM	0.454516 ± 0.280174	1.69802 ± 0.840083	0.813442 ± 0.00720691	0.650227 ± 0.00138861
Gaussian Ensemble + Selective Ens Var	0.226352 ± 0.0677413	0.972076 ± 0.118477	0.701301 ± 0.0146886	0.7711 ± 0.0191172

Table A17: Miscoverage rate $\alpha = 0.2$: Results on the VENTRICULARVOLUME dataset.

Method	val MAE (\downarrow)	val Interval Length (\downarrow)	test Coverage (≥ 0.80)	test Prediction Rate (\uparrow)
Conformal Prediction	11.2471 ± 0.201399	33.0996 ± 0.991594	0.457053 ± 0.00583106	1.0
Gaussian	12.7238 ± 1.52197	37.3172 ± 4.91536	0.589342 ± 0.0793156	1.0
Gaussian Ensemble	10.1141 ± 0.180661	29.9914 ± 1.12007	0.678527 ± 0.0277009	1.0
Quantile Regression	12.5465 ± 0.941364	35.8073 ± 1.5139	0.537774 ± 0.0444887	1.0
Gaussian + Selective GMM	12.7238 ± 1.52197	37.3172 ± 4.91536	0.609177 ± 0.0682058	0.709875 ± 0.0232873
Gaussian Ensemble + Selective Ens Var	10.1141 ± 0.180661	29.9914 ± 1.12007	0.640078 ± 0.0277429	0.686207 ± 0.0431835

Table A18: Miscoverage rate $\alpha = 0.2$: Results on the BRAINTUMOURPIXELS dataset.

Method	val MAE (\downarrow)	val Interval Length (\downarrow)	test Coverage (≥ 0.80)	test Prediction Rate (\uparrow)
Conformal Prediction	21.3163 ± 0.45997	66.146 ± 2.75637	0.824632 ± 0.0128289	1.0
Gaussian	21.0625 ± 0.358012	64.2423 ± 1.9975	0.798113 ± 0.0133438	1.0
Gaussian Ensemble	20.5336 ± 0.211421	62.5706 ± 0.713494	0.796961 ± 0.00658989	1.0
Quantile Regression	21.9545 ± 0.149787	66.2654 ± 1.33091	0.807646 ± 0.0165337	1.0
Gaussian + Selective GMM	21.0625 ± 0.358012	64.2423 ± 1.9975	0.809477 ± 0.0139729	0.973576 ± 0.0187252
Gaussian Ensemble + Selective Ens Var	20.5336 ± 0.211421	62.5706 ± 0.713494	0.806998 ± 0.00641546	0.975368 ± 0.00323397

Table A19: Miscoverage rate $\alpha = 0.2$: Results on the SKINLESIONPIXELS dataset.

Method	val MAE (\downarrow)	val Interval Length (\downarrow)	test Coverage (≥ 0.80)	test Prediction Rate (\uparrow)
Conformal Prediction	107.514 ± 1.87464	275.494 ± 5.60123	0.553254 ± 0.0122434	1.0
Gaussian	105.417 ± 1.15178	395.661 ± 174.897	0.689951 ± 0.0406148	1.0
Gaussian Ensemble	100.639 ± 0.464183	351.961 ± 70.4308	0.715272 ± 0.0278757	1.0
Quantile Regression	106.382 ± 2.70593	251.346 ± 8.67954	0.590792 ± 0.0115523	1.0
Gaussian + Selective GMM	105.417 ± 1.15178	395.661 ± 174.897	0.708767 ± 0.0274691	0.849668 ± 0.0189464
Gaussian Ensemble + Selective Ens Var	100.639 ± 0.464183	351.961 ± 70.4308	0.704273 ± 0.0198608	0.782116 ± 0.0109776

Table A20: Miscoverage rate $\alpha = 0.2$: Results on the HISTOLOGYNUCLEIPIXELS dataset.

Method	val MAE (\downarrow)	val Interval Length (\downarrow)	test Coverage (≥ 0.80)	test Prediction Rate (\uparrow)
Conformal Prediction	217.887 ± 3.71766	688.269 ± 13.6761	0.744155 ± 0.0107073	1.0
Gaussian	211.795 ± 10.0239	902.884 ± 295.983	0.454345 ± 0.0986975	1.0
Gaussian Ensemble	196.785 ± 2.14454	840.287 ± 113.005	0.412528 ± 0.0544736	1.0
Quantile Regression	221.136 ± 9.7918	679.117 ± 30.6895	0.580503 ± 0.0463751	1.0
Gaussian + Selective GMM	211.795 ± 10.0239	902.884 ± 295.983	0.462248 ± 0.105935	0.901985 ± 0.0400294
Gaussian Ensemble + Selective Ens Var	196.785 ± 2.14454	840.287 ± 113.005	0.417977 ± 0.0572495	0.954477 ± 0.0256246

Table A21: Miscoverage rate $\alpha = 0.2$: Results on the AERIALBUILDINGPIXELS dataset.

Method	val MAE (\downarrow)	val Interval Length (\downarrow)	test Coverage (≥ 0.80)	test Prediction Rate (\uparrow)
Conformal Prediction	235.417 ± 7.16096	685.829 ± 31.3669	0.52437 ± 0.0610316	1.0
Gaussian	217.877 ± 1.72493	685.899 ± 43.1749	0.60129 ± 0.0717427	1.0
Gaussian Ensemble	208.487 ± 1.03581	658.243 ± 27.1206	0.683599 ± 0.0674139	1.0
Quantile Regression	229.243 ± 6.21038	662.104 ± 18.5495	0.635733 ± 0.0350343	1.0
Gaussian + Selective GMM	217.877 ± 1.72493	685.899 ± 43.1749	0.679246 ± 0.0462652	0.65018 ± 0.0999173
Gaussian Ensemble + Selective Ens Var	208.487 ± 1.03581	658.243 ± 27.1206	0.743714 ± 0.0354023	0.571928 ± 0.0402727

Table A22: Miscoverage rate $\alpha = 0.05$: Results on the CELLS dataset.

Method	val MAE (\downarrow)	val Interval Length (\downarrow)	test Coverage (≥ 0.95)	test Prediction Rate (\uparrow)
Conformal Prediction	4.03121 ± 2.78375	22.3973 ± 12.7194	0.95612 ± 0.00460235	1.0
Gaussian	3.61704 ± 1.13624	17.0459 ± 4.98381	0.95402 ± 0.00275928	1.0
Gaussian Ensemble	2.78757 ± 1.16951	20.5445 ± 5.00176	0.9484 ± 0.00331843	1.0
Quantile Regression	3.5478 ± 1.25834	17.8244 ± 3.57608	0.94858 ± 0.00565346	1.0
Gaussian + Selective GMM	3.61704 ± 1.13624	17.0459 ± 4.98381	0.955558 ± 0.0032579	0.95212 ± 0.00276362
Gaussian Ensemble + Selective Ens Var	2.78757 ± 1.16951	20.5445 ± 5.00176	0.946085 ± 0.00337562	0.95156 ± 0.00215277

Table A23: Miscoverage rate $\alpha = 0.05$: Results on the CELLS-TAILS dataset.

Method	val MAE (\downarrow)	val Interval Length (\downarrow)	test Coverage (≥ 0.95)	test Prediction Rate (\uparrow)
Conformal Prediction	3.56733 ± 1.0818	16.3831 ± 4.80611	0.59048 ± 0.0307226	1.0
Gaussian	4.05446 ± 1.33153	17.5443 ± 5.3978	0.59066 ± 0.0417946	1.0
Gaussian Ensemble	2.40691 ± 0.580524	13.1205 ± 1.81604	0.67218 ± 0.0308246	1.0
Quantile Regression	3.34375 ± 0.642763	14.5539 ± 2.01592	0.5666 ± 0.0295055	1.0
Gaussian + Selective GMM	4.05446 ± 1.33153	17.5443 ± 5.3978	0.941551 ± 0.0164539	0.53636 ± 0.0100057
Gaussian Ensemble + Selective Ens Var	2.40691 ± 0.580524	13.1205 ± 1.81604	0.720221 ± 0.0374625	0.74512 ± 0.0438128

Table A24: Miscoverage rate $\alpha = 0.05$: Results on the CHAIRANGLE dataset.

Method	val MAE (\downarrow)	val Interval Length (\downarrow)	test Coverage (≥ 0.95)	test Prediction Rate (\uparrow)
Conformal Prediction	0.289127 ± 0.081643	1.27437 ± 0.18759	0.953087 ± 0.000729425	1.0
Gaussian	0.376692 ± 0.171928	1.59112 ± 0.367248	0.949381 ± 0.00143361	1.0
Gaussian Ensemble	0.361834 ± 0.165348	1.38384 ± 0.481345	0.95633 ± 0.0016841	1.0
Quantile Regression	0.888707 ± 0.472522	4.04185 ± 1.50356	0.951608 ± 0.00184683	1.0
Gaussian + Selective GMM	0.376692 ± 0.171928	1.59112 ± 0.367248	0.949963 ± 0.00265095	0.97208 ± 0.00166628
Gaussian Ensemble + Selective Ens Var	0.361834 ± 0.165348	1.38384 ± 0.481345	0.9541 ± 0.00167267	0.951359 ± 0.00453556

Table A25: Miscoverage rate $\alpha = 0.05$: Results on the CHAIRANGLE-GAP dataset.

Method	val MAE (\downarrow)	val Interval Length (\downarrow)	test Coverage (≥ 0.95)	test Prediction Rate (\uparrow)
Conformal Prediction	0.35034 ± 0.161819	1.56264 ± 0.582954	0.697817 ± 0.00918537	1.0
Gaussian	0.454516 ± 0.280174	2.39892 ± 1.02472	0.733595 ± 0.0367327	1.0
Gaussian Ensemble	0.226352 ± 0.0677413	1.59703 ± 0.159795	0.780615 ± 0.0141415	1.0
Quantile Regression	1.43807 ± 0.99796	5.57113 ± 1.71783	0.759929 ± 0.034465	1.0
Gaussian + Selective GMM	0.454516 ± 0.280174	2.39892 ± 1.02472	0.95774 ± 0.00281998	0.64882 ± 0.00276083
Gaussian Ensemble + Selective Ens Var	0.226352 ± 0.0677413	1.59703 ± 0.159795	0.844587 ± 0.0165508	0.7711 ± 0.0191172

Table A26: Miscoverage rate $\alpha = 0.05$: Results on the VENTRICULARVOLUME dataset.

Method	val MAE (\downarrow)	val Interval Length (\downarrow)	test Coverage (≥ 0.95)	test Prediction Rate (\uparrow)
Conformal Prediction	11.2471 ± 0.201399	70.211 ± 1.37665	0.776176 ± 0.00853621	1.0
Gaussian	12.7238 ± 1.52197	67.1562 ± 6.31002	0.837931 ± 0.0396691	1.0
Gaussian Ensemble	10.1141 ± 0.180661	51.9065 ± 3.94789	0.876646 ± 0.0140944	1.0
Quantile Regression	12.0793 ± 0.130032	61.623 ± 3.04835	0.843574 ± 0.0243659	1.0
Gaussian + Selective GMM	12.7238 ± 1.52197	67.1562 ± 6.31002	0.854302 ± 0.0279176	0.710188 ± 0.0225912
Gaussian Ensemble + Selective Ens Var	10.1141 ± 0.180661	51.9065 ± 3.94789	0.855053 ± 0.0125036	0.686207 ± 0.0431835

Table A27: Miscoverage rate $\alpha = 0.05$: Results on the BRAINTUMOURPIXELS dataset.

Method	val MAE (\downarrow)	val Interval Length (\downarrow)	test Coverage (≥ 0.95)	test Prediction Rate (\uparrow)
Conformal Prediction	21.3163 ± 0.45997	123.719 ± 2.07495	0.921113 ± 0.00123648	1.0
Gaussian	21.0625 ± 0.358012	123.587 ± 3.3168	0.910141 ± 0.00537523	1.0
Gaussian Ensemble	20.5336 ± 0.211421	113.592 ± 1.37398	0.905182 ± 0.00359141	1.0
Quantile Regression	24.6897 ± 2.49388	126.788 ± 7.00165	0.915995 ± 0.00956349	1.0
Gaussian + Selective GMM	21.0625 ± 0.358012	123.587 ± 3.3168	0.919455 ± 0.0105219	0.973672 ± 0.0186442
Gaussian Ensemble + Selective Ens Var	20.5336 ± 0.211421	113.592 ± 1.37398	0.91095 ± 0.00267557	0.975368 ± 0.00323397

Table A28: Miscoverage rate $\alpha = 0.05$: Results on the SKINLESIONPIXELS dataset.

Method	val MAE (\downarrow)	val Interval Length (\downarrow)	test Coverage (≥ 0.95)	test Prediction Rate (\uparrow)
Conformal Prediction	107.514 ± 1.87464	845.109 ± 31.2572	0.822753 ± 0.0104666	1.0
Gaussian	105.417 ± 1.15178	691.768 ± 232.071	0.866844 ± 0.0166304	1.0
Gaussian Ensemble	100.639 ± 0.464183	582.719 ± 95.3488	0.881009 ± 0.00686587	1.0
Quantile Regression	112.07 ± 5.13986	627.938 ± 68.3371	0.827977 ± 0.017595	1.0
Gaussian + Selective GMM	105.417 ± 1.15178	691.768 ± 232.071	0.889891 ± 0.00940058	0.849225 ± 0.0194809
Gaussian Ensemble + Selective Ens Var	100.639 ± 0.464183	582.719 ± 95.3488	0.881749 ± 0.00534917	0.782116 ± 0.0109776

Table A29: Miscoverage rate $\alpha = 0.05$: Results on the HISTOLOGYNUCLEIPIXELS dataset.

Method	val MAE (\downarrow)	val Interval Length (\downarrow)	test Coverage (≥ 0.95)	test Prediction Rate (\uparrow)
Conformal Prediction	217.887 ± 3.71766	1282.78 ± 25.9915	0.896603 ± 0.0113207	1.0
Gaussian	211.795 ± 10.0239	1491.62 ± 472.378	0.680018 ± 0.0860417	1.0
Gaussian Ensemble	196.785 ± 2.14454	1358.12 ± 174.189	0.66749 ± 0.0522544	1.0
Quantile Regression	251.562 ± 12.244	1191.96 ± 65.3122	0.754566 ± 0.0379023	1.0
Gaussian + Selective GMM	211.795 ± 10.0239	1491.62 ± 472.378	0.68897 ± 0.0895173	0.901191 ± 0.0405698
Gaussian Ensemble + Selective Ens Var	196.785 ± 2.14454	1358.12 ± 174.189	0.673945 ± 0.0533738	0.954477 ± 0.0256246

Table A30: Miscoverage rate $\alpha = 0.05$: Results on the AERIALBUILDINGPIXELS dataset.

Method	val MAE (\downarrow)	val Interval Length (\downarrow)	test Coverage (≥ 0.95)	test Prediction Rate (\uparrow)
Conformal Prediction	235.417 ± 7.16096	1474.93 ± 53.6301	0.731414 ± 0.070291	1.0
Gaussian	217.877 ± 1.72493	1181.55 ± 41.5859	0.773522 ± 0.0548329	1.0
Gaussian Ensemble	208.487 ± 1.03581	1108.87 ± 21.3551	0.88874 ± 0.0490213	1.0
Quantile Regression	294.181 ± 19.9268	1281.37 ± 51.1001	0.888175 ± 0.028968	1.0
Gaussian + Selective GMM	217.877 ± 1.72493	1181.55 ± 41.5859	0.831501 ± 0.0374173	0.650797 ± 0.0987431
Gaussian Ensemble + Selective Ens Var	208.487 ± 1.03581	1108.87 ± 21.3551	0.899838 ± 0.0263409	0.571928 ± 0.0402727

Table A31: Method variation results on the CELLS dataset.

Method	val MAE (\downarrow)	val Interval Length (\downarrow)	test Coverage (≥ 0.90)	test Prediction Rate (\uparrow)
Gaussian + Selective GMM	3.61704 ± 1.13624	14.5492 ± 4.44927	0.905241 ± 0.00448315	0.95216 ± 0.00290558
Gaussian + Selective GMM, $k = 2$	3.61704 ± 1.13624	14.5492 ± 4.44927	0.9044 ± 0.00481955	0.952 ± 0.00270259
Gaussian + Selective GMM, $k = 8$	3.61704 ± 1.13624	14.5492 ± 4.44927	0.904928 ± 0.00469093	0.9528 ± 0.00331662
Gaussian + Selective GMM, Spectral Norm	4.80289 ± 1.89759	18.5596 ± 9.13391	0.908 ± 0.00703097	0.95118 ± 0.00220672
Gaussian + Selective kNN	3.61704 ± 1.13624	14.5492 ± 4.44927	0.900069 ± 0.00677637	0.94656 ± 0.00470472
Gaussian + Selective kNN, $k = 5$	3.61704 ± 1.13624	14.5492 ± 4.44927	0.900146 ± 0.00671325	0.94736 ± 0.00395049
Gaussian + Selective kNN, $k = 20$	3.61704 ± 1.13624	14.5492 ± 4.44927	0.900048 ± 0.00691667	0.94624 ± 0.00248564
Gaussian + Selective kNN, L2	3.61704 ± 1.13624	14.5492 ± 4.44927	0.906295 ± 0.00579854	0.95166 ± 0.00422734

Table A32: Method variation results on the CELLS-TAILS dataset.

Method	val MAE (\downarrow)	val Interval Length (\downarrow)	test Coverage (≥ 0.90)	test Prediction Rate (\uparrow)
Gaussian + Selective GMM	4.05446 ± 1.33153	15.4321 ± 4.98796	0.889825 ± 0.0193021	0.53654 ± 0.0101012
Gaussian + Selective GMM, $k = 2$	4.05446 ± 1.33153	15.4321 ± 4.98796	0.891933 ± 0.0175265	0.525 ± 0.00829409
Gaussian + Selective GMM, $k = 8$	4.05446 ± 1.33153	15.4321 ± 4.98796	0.893648 ± 0.0182098	0.53516 ± 0.00975635
Gaussian + Selective GMM, Spectral Norm	4.91114 ± 2.46961	17.3945 ± 7.3177	0.881351 ± 0.021587	0.5331 ± 0.0157885
Gaussian + Selective kNN	4.05446 ± 1.33153	15.4321 ± 4.98796	0.859179 ± 0.0255173	0.56692 ± 0.0127107
Gaussian + Selective kNN, $k = 5$	4.05446 ± 1.33153	15.4321 ± 4.98796	0.855387 ± 0.0261636	0.57206 ± 0.0129226
Gaussian + Selective kNN, $k = 20$	4.05446 ± 1.33153	15.4321 ± 4.98796	0.862429 ± 0.0264602	0.56236 ± 0.0122017
Gaussian + Selective kNN, L2	4.05446 ± 1.33153	15.4321 ± 4.98796	0.898932 ± 0.00921808	0.51486 ± 0.00474662

Table A33: Method variation results on the CELLS-GAP dataset.

Method	val MAE (\downarrow)	val Interval Length (\downarrow)	test Coverage (≥ 0.90)	test Prediction Rate (\uparrow)
Gaussian + Selective GMM	3.53089 \pm 0.0619	15.6396 \pm 6.23458	0.890569 \pm 0.00953089	0.49372 \pm 0.0025926
Gaussian + Selective GMM, $k = 2$	3.53089 \pm 0.0619	15.6396 \pm 6.23458	0.892265 \pm 0.00867262	0.48902 \pm 0.00420828
Gaussian + Selective GMM, $k = 8$	3.53089 \pm 0.0619	15.6396 \pm 6.23458	0.88967 \pm 0.0111239	0.50196 \pm 0.00492041
Gaussian + Selective GMM, Spectral Norm	2.81679 \pm 0.42988	12.194 \pm 1.10907	0.883644 \pm 0.0167566	0.4991 \pm 0.00761236
Gaussian + Selective kNN	3.53089 \pm 0.0619	15.6396 \pm 6.23458	0.874032 \pm 0.0432364	0.53646 \pm 0.0139864
Gaussian + Selective kNN, $k = 5$	3.53089 \pm 0.0619	15.6396 \pm 6.23458	0.874822 \pm 0.0424219	0.5368 \pm 0.0137332
Gaussian + Selective kNN, $k = 20$	3.53089 \pm 0.0619	15.6396 \pm 6.23458	0.873876 \pm 0.0443446	0.536 \pm 0.014724
Gaussian + Selective kNN, L2	3.53089 \pm 0.0619	15.6396 \pm 6.23458	0.887052 \pm 0.0144573	0.49576 \pm 0.00474578

Table A34: Method variation results on the CHAIRANGLE dataset.

Method	val MAE (\downarrow)	val Interval Length (\downarrow)	test Coverage (≥ 0.90)	test Prediction Rate (\uparrow)
Gaussian + Selective GMM	0.376692 \pm 0.171928	1.37757 \pm 0.382191	0.902482 \pm 0.00436054	0.972739 \pm 0.00191733
Gaussian + Selective GMM, $k = 2$	0.376692 \pm 0.171928	1.37757 \pm 0.382191	0.902972 \pm 0.00540708	0.96392 \pm 0.00121759
Gaussian + Selective GMM, $k = 8$	0.376692 \pm 0.171928	1.37757 \pm 0.382191	0.901822 \pm 0.00328732	0.981238 \pm 0.00113892
Gaussian + Selective GMM, Spectral Norm	0.516487 \pm 0.227015	1.82929 \pm 0.809339	0.903828 \pm 0.00534803	0.970993 \pm 0.000466666
Gaussian + Selective kNN	0.376692 \pm 0.171928	1.37757 \pm 0.382191	0.90222 \pm 0.00459694	0.975465 \pm 0.00201785
Gaussian + Selective kNN, $k = 5$	0.376692 \pm 0.171928	1.37757 \pm 0.382191	0.902561 \pm 0.00342563	0.983804 \pm 0.00152586
Gaussian + Selective kNN, $k = 20$	0.376692 \pm 0.171928	1.37757 \pm 0.382191	0.902137 \pm 0.00457917	0.966592 \pm 0.00129222
Gaussian + Selective kNN, L2	0.376692 \pm 0.171928	1.37757 \pm 0.382191	0.903183 \pm 0.00504343	0.977247 \pm 0.00149241

Table A35: Method variation results on the CHAIRANGLE-TAILS dataset.

Method	val MAE (\downarrow)	val Interval Length (\downarrow)	test Coverage (≥ 0.90)	test Prediction Rate (\uparrow)
Gaussian + Selective GMM	0.241214 \pm 0.091736	1.09417 \pm 0.382907	0.901946 \pm 0.00382993	0.655448 \pm 0.001058
Gaussian + Selective GMM, $k = 2$	0.241214 \pm 0.091736	1.09417 \pm 0.382907	0.903353 \pm 0.00471599	0.645452 \pm 0.00155062
Gaussian + Selective GMM, $k = 8$	0.241214 \pm 0.091736	1.09417 \pm 0.382907	0.902103 \pm 0.00382668	0.660472 \pm 0.00115112
Gaussian + Selective GMM, Spectral Norm	0.375118 \pm 0.24509	1.24343 \pm 0.611561	0.910147 \pm 0.00315697	0.65518 \pm 0.00176257
Gaussian + Selective kNN	0.241214 \pm 0.091736	1.09417 \pm 0.382907	0.860311 \pm 0.00617031	0.703038 \pm 0.00691227
Gaussian + Selective kNN, $k = 5$	0.241214 \pm 0.091736	1.09417 \pm 0.382907	0.88625 \pm 0.00498864	0.683742 \pm 0.00547083
Gaussian + Selective kNN, $k = 20$	0.241214 \pm 0.091736	1.09417 \pm 0.382907	0.809551 \pm 0.00764886	0.743287 \pm 0.0107676
Gaussian + Selective kNN, L2	0.241214 \pm 0.091736	1.09417 \pm 0.382907	0.89682 \pm 0.00698641	0.662076 \pm 0.00289246

Table A36: Method variation results on the CHAIRANGLE-GAP dataset.

Method	val MAE (\downarrow)	val Interval Length (\downarrow)	test Coverage (≥ 0.90)	test Prediction Rate (\uparrow)
Gaussian + Selective GMM	0.454516 \pm 0.280174	2.09212 \pm 0.933756	0.91215 \pm 0.00604745	0.649372 \pm 0.00334919
Gaussian + Selective GMM, $k = 2$	0.454516 \pm 0.280174	2.09212 \pm 0.933756	0.912708 \pm 0.00541793	0.642138 \pm 0.00143869
Gaussian + Selective GMM, $k = 8$	0.454516 \pm 0.280174	2.09212 \pm 0.933756	0.911374 \pm 0.00475979	0.654824 \pm 0.00368979
Gaussian + Selective GMM, Spectral Norm	0.294511 \pm 0.0861797	1.19904 \pm 0.193646	0.910836 \pm 0.00442911	0.649996 \pm 0.00233428
Gaussian + Selective kNN	0.454516 \pm 0.280174	2.09212 \pm 0.933756	0.911574 \pm 0.00376608	0.673764 \pm 0.0113432
Gaussian + Selective kNN, $k = 5$	0.454516 \pm 0.280174	2.09212 \pm 0.933756	0.91224 \pm 0.00426519	0.670646 \pm 0.00691764
Gaussian + Selective kNN, $k = 20$	0.454516 \pm 0.280174	2.09212 \pm 0.933756	0.907543 \pm 0.00204724	0.680107 \pm 0.0162927
Gaussian + Selective kNN, L2	0.454516 \pm 0.280174	2.09212 \pm 0.933756	0.913383 \pm 0.00539352	0.658744 \pm 0.00274677

Table A37: Method variation results on the ASSETWEALTH dataset.

Method	val MAE (\downarrow)	val Interval Length (\downarrow)	test Coverage (≥ 0.90)	test Prediction Rate (\uparrow)
Gaussian + Selective GMM	0.367501 \pm 0.0416437	1.597 \pm 0.207599	0.850824 \pm 0.047533	0.93838 \pm 0.0170443
Gaussian + Selective GMM, $k = 2$	0.367501 \pm 0.0416437	1.597 \pm 0.207599	0.850232 \pm 0.0469534	0.933687 \pm 0.0176348
Gaussian + Selective GMM, $k = 8$	0.367501 \pm 0.0416437	1.597 \pm 0.207599	0.85067 \pm 0.0456954	0.932879 \pm 0.0102523
Gaussian + Selective GMM, Spectral Norm	0.354467 \pm 0.00973911	1.55594 \pm 0.0421589	0.872742 \pm 0.0250168	0.941812 \pm 0.0101895
Gaussian + Selective kNN	0.367501 \pm 0.0416437	1.597 \pm 0.207599	0.852107 \pm 0.0474734	0.933586 \pm 0.0203541
Gaussian + Selective kNN, $k = 5$	0.367501 \pm 0.0416437	1.597 \pm 0.207599	0.85256 \pm 0.0469571	0.933232 \pm 0.02149
Gaussian + Selective kNN, $k = 20$	0.367501 \pm 0.0416437	1.597 \pm 0.207599	0.851914 \pm 0.0460655	0.933636 \pm 0.0200087
Gaussian + Selective kNN, L2	0.367501 \pm 0.0416437	1.597 \pm 0.207599	0.853365 \pm 0.0410864	0.897149 \pm 0.0162693

Table A38: Method variation results on the VENTRICULARVOLUME dataset.

Method	val MAE (\downarrow)	val Interval Length (\downarrow)	test Coverage (≥ 0.90)	test Prediction Rate (\uparrow)
Gaussian + Selective GMM	12.7238 \pm 1.52197	51.566 \pm 3.52739	0.752046 \pm 0.0529087	0.707994 \pm 0.0208741
Gaussian + Selective GMM, $k = 2$	12.7238 \pm 1.52197	51.566 \pm 3.52739	0.745271 \pm 0.0582068	0.790752 \pm 0.0307666
Gaussian + Selective GMM, $k = 8$	12.7238 \pm 1.52197	51.566 \pm 3.52739	0.747625 \pm 0.0584117	0.656583 \pm 0.0258853
Gaussian + Selective GMM, Spectral Norm	11.6311 \pm 0.483357	45.5475 \pm 0.747647	0.734907 \pm 0.00853342	0.719279 \pm 0.0147984
Gaussian + Selective kNN	12.7238 \pm 1.52197	51.566 \pm 3.52739	0.735105 \pm 0.0612413	0.911599 \pm 0.0447475
Gaussian + Selective kNN, $k = 5$	12.7238 \pm 1.52197	51.566 \pm 3.52739	0.735857 \pm 0.0604531	0.916614 \pm 0.0419073
Gaussian + Selective kNN, $k = 20$	12.7238 \pm 1.52197	51.566 \pm 3.52739	0.734752 \pm 0.0616982	0.909404 \pm 0.0469634
Gaussian + Selective kNN, L2	12.7238 \pm 1.52197	51.566 \pm 3.52739	0.740812 \pm 0.049802	0.740439 \pm 0.0222073

Table A39: Method variation results on the BRAINTUMOURPIXELS dataset.

Method	val MAE (\downarrow)	val Interval Length (\downarrow)	test Coverage (≥ 0.90)	test Prediction Rate (\uparrow)
Gaussian + Selective GMM	21.0625 \pm 0.358012	93.6284 \pm 2.29916	0.883515 \pm 0.0138279	0.973576 \pm 0.0187252
Gaussian + Selective GMM, $k = 2$	21.0625 \pm 0.358012	93.6284 \pm 2.29916	0.881874 \pm 0.0118346	0.977863 \pm 0.0145103
Gaussian + Selective GMM, $k = 8$	21.0625 \pm 0.358012	93.6284 \pm 2.29916	0.880823 \pm 0.01273	0.973417 \pm 0.01856
Gaussian + Selective GMM, Spectral Norm	22.0729 \pm 1.25273	95.0605 \pm 3.40124	0.890506 \pm 0.0112498	0.9738 \pm 0.00857087
Gaussian + Selective kNN	21.0625 \pm 0.358012	93.6284 \pm 2.29916	0.891264 \pm 0.00734602	0.947185 \pm 0.0178434
Gaussian + Selective kNN, $k = 5$	21.0625 \pm 0.358012	93.6284 \pm 2.29916	0.891103 \pm 0.00680399	0.949392 \pm 0.0173229
Gaussian + Selective kNN, $k = 20$	21.0625 \pm 0.358012	93.6284 \pm 2.29916	0.891759 \pm 0.00804523	0.94453 \pm 0.0188456
Gaussian + Selective kNN, L2	21.0625 \pm 0.358012	93.6284 \pm 2.29916	0.879639 \pm 0.0084247	0.981862 \pm 0.0068585

Table A40: Method variation results on the SKINLESIONPIXELS dataset.

Method	val MAE (\downarrow)	val Interval Length (\downarrow)	test Coverage (≥ 0.90)	test Prediction Rate (\uparrow)
Gaussian + Selective GMM	105.417 \pm 1.15178	535.139 \pm 215.446	0.821515 \pm 0.0137705	0.849579 \pm 0.0206181
Gaussian + Selective GMM, $k = 2$	105.417 \pm 1.15178	535.139 \pm 215.446	0.825054 \pm 0.0122698	0.844799 \pm 0.0191092
Gaussian + Selective GMM, $k = 8$	105.417 \pm 1.15178	535.139 \pm 215.446	0.815696 \pm 0.010454	0.862683 \pm 0.0259293
Gaussian + Selective GMM, Spectral Norm	107.531 \pm 2.11824	607.435 \pm 407.758	0.821797 \pm 0.0350093	0.837273 \pm 0.0205022
Gaussian + Selective kNN	105.417 \pm 1.15178	535.139 \pm 215.446	0.813027 \pm 0.0306586	0.927047 \pm 0.00830718
Gaussian + Selective kNN, $k = 5$	105.417 \pm 1.15178	535.139 \pm 215.446	0.812763 \pm 0.0309198	0.928375 \pm 0.0100103
Gaussian + Selective kNN, $k = 20$	105.417 \pm 1.15178	535.139 \pm 215.446	0.812419 \pm 0.0306294	0.929172 \pm 0.0109976
Gaussian + Selective kNN, L2	105.417 \pm 1.15178	535.139 \pm 215.446	0.808667 \pm 0.0112832	0.831784 \pm 0.0181658

Table A41: Method variation results on the HISTOLOGYNUCLEIPIXELS dataset.

Method	val MAE (\downarrow)	val Interval Length (\downarrow)	test Coverage (≥ 0.90)	test Prediction Rate (\uparrow)
Gaussian + Selective GMM	211.795 \pm 10.0239	1211.83 \pm 396.946	0.59554 \pm 0.0956742	0.90569 \pm 0.0453555
Gaussian + Selective GMM, $k = 2$	211.795 \pm 10.0239	1211.83 \pm 396.946	0.597998 \pm 0.094508	0.912836 \pm 0.0323147
Gaussian + Selective GMM, $k = 8$	211.795 \pm 10.0239	1211.83 \pm 396.946	0.595718 \pm 0.0973458	0.943449 \pm 0.0409511
Gaussian + Selective GMM, Spectral Norm	206.492 \pm 7.82601	896.779 \pm 61.4921	0.65672 \pm 0.0824111	0.855668 \pm 0.0632114
Gaussian + Selective kNN	211.795 \pm 10.0239	1211.83 \pm 396.946	0.608929 \pm 0.0805954	0.846228 \pm 0.0482832
Gaussian + Selective kNN, $k = 5$	211.795 \pm 10.0239	1211.83 \pm 396.946	0.610025 \pm 0.0809455	0.842258 \pm 0.046231
Gaussian + Selective kNN, $k = 20$	211.795 \pm 10.0239	1211.83 \pm 396.946	0.607876 \pm 0.0817183	0.858491 \pm 0.0496696
Gaussian + Selective kNN, L2	211.795 \pm 10.0239	1211.83 \pm 396.946	0.588514 \pm 0.0914286	0.975562 \pm 0.0190356

Table A42: Method variation results on the AERIALBUILDINGPIXELS dataset.

Method	val MAE (\downarrow)	val Interval Length (\downarrow)	test Coverage (≥ 0.90)	test Prediction Rate (\uparrow)
Gaussian + Selective GMM	217.877 \pm 1.72493	929.562 \pm 47.6606	0.76535 \pm 0.0388677	0.652082 \pm 0.0990489
Gaussian + Selective GMM, $k = 2$	217.877 \pm 1.72493	929.562 \pm 47.6606	0.751721 \pm 0.0454772	0.634602 \pm 0.122618
Gaussian + Selective GMM, $k = 8$	217.877 \pm 1.72493	929.562 \pm 47.6606	0.850213 \pm 0.025791	0.617738 \pm 0.0879951
Gaussian + Selective GMM, Spectral Norm	220.763 \pm 7.23119	1014.77 \pm 164.155	0.817517 \pm 0.0505544	0.638149 \pm 0.046255
Gaussian + Selective kNN	217.877 \pm 1.72493	929.562 \pm 47.6606	0.651867 \pm 0.0771154	0.840103 \pm 0.0463989
Gaussian + Selective kNN, $k = 5$	217.877 \pm 1.72493	929.562 \pm 47.6606	0.654256 \pm 0.0771566	0.846067 \pm 0.0456245
Gaussian + Selective kNN, $k = 20$	217.877 \pm 1.72493	929.562 \pm 47.6606	0.647779 \pm 0.0795474	0.832596 \pm 0.0542738
Gaussian + Selective kNN, L2	217.877 \pm 1.72493	929.562 \pm 47.6606	0.815075 \pm 0.0278439	0.641851 \pm 0.11347